A second-order accurate, mass lumped finite element scheme for a ternary time-dependent Ginzburg-Landau system of macromolecular microsphere composite hydrogels

Maoqin Yuan * Lixiu Dong † Cheng Wang‡

December 13, 2025

Abstract

This paper introduces a fully discrete finite element numerical scheme specifically tailored for a ternary time-dependent Ginzburg-Landau-deGennes mesoscopic model, and provides a thorough analysis. The scheme is constructed using the mass-lumped finite element spatial discretization and the second-order Backward Differentiation Formula (BDF2) temporal discretization, ensuring a robust framework for simulation. To effectively handle the highly complicated energy functional, we employ the convex-concave decomposition technique. Meanwhile, an addition of a Douglas-Dupont regularization term allows one to establish a modified energy stability estimate, which is crucial for the theoretical foundation. The unique solvability and positivity-preserving properties of the proposed scheme are rigorously justified, reinforcing its theoretical validity. To validate these theoretical insights and demonstrate the practical applications, a series of numerical experiments are performed, highlighting the evolution of the MMC hydrogel. Notably, the study also delves into the impact of the stability factor on both energy stability and numerical error, providing a comprehensive evaluation of the numerical performance and reliability.

AMS subject classifications: 35K25, 35K55, 60F10, 65M60

Keywords: Flory-Huggins-deGennes energy potential, mass lumped finite element method, second order backward differentiation formula (BDF2), energy stability analysis, positivity preserving property

1 Introduction

Hydrogels, which are networks composed of cross-linked hydrophilic polymer chains, boast a remarkably broad range of applications. These versatile materials are extensively utilized in

*Department of Mathematics, School of Science and Art, China University of Petroleum-Beijing at Karamay, Karamay 834000, P.R. China(mqyuan@cupk.edu.cn).

†Department of Mathematics, Faculty of Arts and Sciences, Beijing Normal University, Zhuhai 519087, P.R. China(Corresponding Author: lxdong@bnu.edu.cn).

‡Department of Mathematics, University of Massachusetts, North Dartmouth, MA 02747, USA (cwang1@umassd.edu).

various areas, including drug delivery system, biosensor, wound dressing, contact lense, and so on [19, 39]. Macromolecular microsphere composite (MMC) hydrogels have garnered significant attention within the realm of polymeric materials. This is attributable to their exceptional high mechanical strength and well-defined network microstructures, as documented in the research by Huang et al. [26]. Their unique attributes render MMC hydrogels a promising candidate for a variety of advanced applications, further propelling the interest and research efforts in this domain. There exist various models to describe the evolution of the MMC hydrogel. In [46], the authors have used the time-dependent Ginzburg-Landau mesoscale (TDGL) model to describe the periodic structure and the phase transition of the MMC hydrogels, and named it as the binary MMC-TDGL equation. Some numerical methods have been reported as well, such as semi-implicit finite difference scheme [29, 30], stabilized method [42], convex-splitting finite difference method [16] and mass-lumped approximation method [24], etc. In [27], Ji et al. proposed an improved model known as the ternary MMC-TDGL system, where graft chains are randomly distributed around macromolecular microsphere. That is to say, polymer chains, the macromolecular microsphere, and solvent are regarded as the three components of the phase transition model in the MMC hydrogels. This turns out to be a more practical system to simulate the phase transition process of MMC hydrogels, and it is able to describe certain phenomena observed in chemical experiments. The ternary MMC-TDGL system features the following Flory-Huggins-deGennes energy potential:

$$F_o(\phi_1,\phi_2,\phi_3)=\int_\Omega \{S_o(\phi_1,\phi_2,\phi_3)+H_o(\phi_1,\phi_2,\phi_3)+K_o(\phi_1,\phi_2,\phi_3)\}\,d\mathbf{x},$$

where $S_o(\phi_1,\phi_2,\phi_3)+H_o(\phi_1,\phi_2,\phi_3)$ is the reticular free energy density:

$$\begin{aligned}S_o(\phi_1,\phi_2,\phi_3)&=\frac{\phi_1}{\gamma}\ln\left(\frac{\alpha\phi_1}{\gamma}\right)+\frac{\phi_2}{N}\ln\left(\frac{\beta\phi_2}{N}\right)+\phi_3\ln\phi_3,\\ H_o(\phi_1,\phi_2,\phi_3)&=\chi_{12}\phi_1\phi_2+\chi_{13}\phi_1\phi_3+\chi_{23}\phi_2\phi_3.\end{aligned}$$

In this system, $K_o(\phi_1,\phi_2,\phi_3)=\frac{1}{36}\sum_{i=1}^{3}a_i^2|\nabla\phi_i|^2/\phi_i$ is the interfacial energy density, a_i is the statistical segment length of the i^{th} component, which is always positive. The phase variable $\phi_i(\mathbf{x},t)$ is the spatiotemporal concentration of component i, with $i=1,2,3$, where $\mathbf{x}$ lies in $\Omega=[0,L_x]\times[0,L_y]\subset\mathbb{R}^2$, an open bounded, connected domain. Concretely, the unknown phase variable ϕ_1,ϕ_2 and ϕ_3 are conserved field variables, representing the concentration of the macromolecular microsphere, the concentration of the polymer chain, and the concentration of the solvent, respectively. These three phase variables are subject to the "no-voids" constraint $\phi_1+\phi_2+\phi_3=1$. In the reticular free energy density distribution, S_o is often called the ideal solution part, and H_o refers to the entropy of mixing part. The sum S_o+H_o is also denoted as the regular solution model in material science and the Flory-Huggins model in polymer chemistry. The parameter α and β are determined by the following formula: $\alpha=\pi(\sqrt{\gamma/\pi}+N/2)^2,\ \beta=2\sqrt{\gamma/\pi}+N$, where the parameter γ is the relative volume of one macromolecular microsphere, and the parameter N stands for the degree of polymerization of the polymer chains. The symbols χ_{12},χ_{13}, and χ_{23} are employed to signify the Huggins interaction parameters corresponding to the interactions between: (i) macromolecular microspheres and polymer chains, (ii) macromolecular microspheres and solvent, and (iii) polymer chains and solvent, respectively. It is noteworthy that these parameters are strictly positive, reflecting the nature of the interactions under consideration.

Making use of the no-voids constraint $\phi_3 = 1-\phi_1-\phi_2$, we can rewrite the energy functional as

$$F(\phi_1,\phi_2)=\int_\Omega \Big\{S(\phi_1,\phi_2)+H(\phi_1,\phi_2)+K(\phi_1,\phi_2)\Big\}d\mathbf{x}, \tag{1.1}$$

where, naturally,

$$\begin{aligned}
S(\phi_1,\phi_2)&=\frac{\phi_1}{\gamma}\ln\left(\frac{\alpha\phi_1}{\gamma}\right)+\frac{\phi_2}{N}\ln\left(\frac{\beta\phi_2}{N}\right)+(1-\phi_1-\phi_2)\ln(1-\phi_1-\phi_2),\\
H(\phi_1,\phi_2)&=\chi_{12}\phi_1\phi_2+\chi_{13}\phi_1(1-\phi_1-\phi_2)+\chi_{23}\phi_2(1-\phi_1-\phi_2),\\
K(\phi_1,\phi_2)&=\frac{a_1^2}{36\phi_1}|\nabla\phi_1|^2+\frac{a_2^2}{36\phi_2}|\nabla\phi_2|^2+\frac{a_3^2}{36(1-\phi_1-\phi_2)}|\nabla(1-\phi_1-\phi_2)|^2.
\end{aligned}$$

In the case of $\phi_1=\phi,\ \phi_2=1-\phi,\ a_1=a_2=a$, the interfacial energy density becomes $K(\phi)=\frac{a_1^2}{36\phi_1}|\nabla\phi_1|^2+\frac{a_2^2}{36\phi_2}|\nabla\phi_2|^2=\frac{a^2}{36\phi(1-\phi)}|\nabla\phi|^2$. The interfacial parameter $\frac{a^2}{36\phi(1-\phi)}$ was proposed by physicist P.G. deGennes for the binary Cahn-Hilliard flow [10]. Therefore, the ternary MMC system turns out to be an obvious extension to the binary case in [46].

Ternary MMC hydrogels dynamic system, corresponding to an H^{-1} gradient flow associated with the given energy functional (1.1), is formulated as

$$\frac{\partial\phi_1}{\partial t}=D_1\Delta\mu_1,\ \frac{\partial\phi_2}{\partial t}=D_2\Delta\mu_2, \tag{1.2}$$

where $D_1,D_2>0$ are mobilities. The chemical potentials μ_1 and μ_2, with respect to ϕ_1 and ϕ_2, respectively, are derived as

$$\begin{aligned}
\mu_1=\frac{\delta F(\phi_1,\phi_2)}{\delta\phi_1}&=\frac{\partial S(\phi_1,\phi_2)}{\partial\phi_1}-\frac{a_1^2|\nabla\phi_1|^2}{36\phi_1^2}-\nabla\cdot\left(\frac{a_1^2\nabla\phi_1}{18\phi_1}\right)+\frac{a_3^2|\nabla(1-\phi_1-\phi_2)|^2}{36(1-\phi_1-\phi_2)^2}\\
&\quad+\nabla\cdot\left(\frac{a_3^2\nabla(1-\phi_1-\phi_2)}{18(1-\phi_1-\phi_2)}\right)+\frac{\partial H(\phi_1,\phi_2)}{\partial\phi_1},\\
\mu_2=\frac{\delta F(\phi_1,\phi_2)}{\delta\phi_2}&=\frac{\partial S(\phi_1,\phi_2)}{\partial\phi_2}-\frac{a_2^2|\nabla\phi_2|^2}{36\phi_2^2}-\nabla\cdot\left(\frac{a_2^2\nabla\phi_2}{18\phi_2}\right)+\frac{a_3^2|\nabla(1-\phi_1-\phi_2)|^2}{36(1-\phi_1-\phi_2)^2}\\
&\quad+\nabla\cdot\left(\frac{a_3^2\nabla(1-\phi_1-\phi_2)}{18(1-\phi_1-\phi_2)}\right)+\frac{\partial H(\phi_1,\phi_2)}{\partial\phi_2},
\end{aligned}$$

in which

$$\begin{aligned}
\frac{\partial S}{\partial\phi_1}&=\frac{1}{\gamma}\ln\left(\frac{\alpha\phi_1}{\gamma}\right)+\frac{1}{\gamma}-1-\ln(1-\phi_1-\phi_2),\quad \frac{\partial H}{\partial\phi_1}=-2\chi_{13}\phi_1+(\chi_{12}-\chi_{13}-\chi_{23})\phi_2+\chi_{13},\\
\frac{\partial S}{\partial\phi_2}&=\frac{1}{N}\ln\left(\frac{\beta\phi_2}{N}\right)+\frac{1}{N}-1-\ln(1-\phi_1-\phi_2),\ \frac{\partial H}{\partial\phi_2}=-2\chi_{23}\phi_2+(\chi_{12}-\chi_{13}-\chi_{23})\phi_1+\chi_{23}.
\end{aligned}$$

This model is characterized as a fourth-order parabolic system of partial differential equations, featuring highly nonlinear terms and singularities within its energy functional. It serves to simulate the intricate phase transition process of macromolecular microsphere composite hydrogels, providing valuable insights into the underlying dynamics of these complex materials. Equipped with periodic boundary conditions, equation (1.2) obviously satisfies the following properties due to the gradient structure: (i) Energy dissipation, i.e., $\frac{dF}{dt}\le 0$; (ii) Mass conservation, i.e., $\int_\Omega\phi_i(\mathbf{x},t)d\mathbf{x}=$

$\int_\Omega \phi_i(\mathbf{x},0)d\mathbf{x}$, with $i = 1,2,3$. Moreover, one well-known theoretical difficulty for the ternary system with logarithmic energy potential is associated with the singularity as the phase variable approaches the limiting values. PDE solutions are anticipative to satisfy a positivity-preserving property, namely, the phase variable ϕ_i remains in the interval $(0,1)$. It is desirable to construct a fully discrete numerical scheme that satisfies these properties.

The ternary MMC hydrogel model is a Cahn-Hilliard-type system. There are various temporal discretization approaches for gradient flows to ensure energy stability. A popular convex splitting method, first proposed by Eyre [20], decomposes the energy functional into the sum of one concave and one convex functionals. In turn, the convex part was treated implicitly and the concave part is computed explicitly. This idea has also been applied to a wide class of gradient flow problems; see the related works for the phase field crustal (PFC) and the modified PFC (MPFC) equations [13, 38], the epitaxial thin-film growth models [22], the Poisson-Nernst-Planck (PNP) [31], and Cahn-Hilliard flow coupled with fluid motion [1, 41], etc. Some other popular energy stabilizing methods have been extensively studied as well, such as the invariant energy quadrant (IEQ) [43], scalar auxiliary variable (SAV) [36], linear stabilization method [28] and Lagrange multiplier approaches [6, 7]. Typically, these methods exhibit stability with respect to a modified form of energy. In recent years, by introducing a supplementary variable to reformulate the original problem as a constrained optimization problem, Hong et al [23] proposed a novel energy-stable scheme that satisfies the original energy dissipation. Ding et al [12] designed a modified Crank-Nicolson method, combined with finite volume spatial discretization, for the modified PNP equations to preserve the original discrete energy dissipation, and this algorithm is suitable for a type of gradient flow problems with entropy of the $\phi \ln \phi$ form.

For the ternary MMC hydrogel system, the first-order [14, 15] and second-order [18] accurate, semi-implicit finite difference schemes have been proposed and analyzed, by incorporating the convex splitting idea. In these finite difference approaches, unique solvability, positivity-preserving properties, unconditional energy stability and convergence analysis have been theoretically justified. Meanwhile, a first-order accurate, mass-lumped finite element numerical method was proposed in [44], while its convergence analysis remains a significant challenge. In fact, one well-known drawback of the first order convex splitting approach is associated with the fact that an extra dissipation added to ensure unconditional stability would cause a significant amount of numerical error [8]. Because of this subtle fact, a high-order accurate, energy stable numerical method has always been highly desirable. At present, most high-order temporal discretization schemes have been constructed for phase-field gradient flows with polynomial energy potential, such as extrapolated Runge-Kutta with scalar auxiliary variable (RK-SAV) method [37, 40], exponential scalar auxiliary variable approaches with relaxation (RE-SAV) [9, 34], the k-th backward differentiation formula (BDFk) [5], etc. On the other hand, the coarsening dynamics is usually a long time process. To improve the computational efficiency, some adaptive time stepping strategy has also become a popular issue for a class of PDEs, and such a strategy is relatively more difficult than the uniform temporal mesh in the theoretical analysis. Some works on the variable-step BDF2 approximation have also been reported, including the ones based on either SAV [9, 25] or convex splitting approach [33]. In terms of the implementation process for the nonlinear numerical schemes, the preconditioned gradient descent (PSD) solver [4, 21, 22] turns out to be an effective approach, due to the fact that most implicit nonlinear terms correspond to a convex energy in the computation of

gradient flows. Meanwhile, as an alternate method, Park et al. [35] has also developed a preconditioned Nesterov's accelerated gradient descent solver for the phase field crystal and functionalized Cahn-Hilliard equations.

The ternary Cahn-Hilliard system (1.2) is much more difficult than the one with polynomial Ginzburg-Landau free energy density potential [2]. Owing to the singular nature of the Flory-Huggins logarithmic free energy density, enforcing the positivity-preserving property for the numerical solution is essential to ensure the well-defined feature of the numerical scheme. However, a mathematical proof of this property turns out to be a very challenging issue. For example, an application of either IEQ [43], SAV [36] or linear stabilization method [28] would not be able to keep such a property, due to an explicit treatment of the nonlinear singular terms. Moreover, the highly nonlinear and singular nature of the surface diffusion coefficients makes the system even more challenging, both analytically and numerically. To address the aforementioned difficulties, we aim to construct and validate a second order accurate numerical scheme for the ternary MMC hydrogel model by employing the convex splitting idea, in combination with the mass-lumped finite element spatial discretization. In comparison with the standard finite element approximation, the mass-lumped method features a diagonal mass matrix, which ensures the point-wise positivity-preserving property of the phase variables. This subtle fact plays a crucial role to ensure the theoretical analysis. Specifically, a second-order BDF (Backward Differentiation Formula) approximation is taken in the temporal discretization, for the sake of second order accuracy. The logarithmic and the interfacial expansion terms are implicitly treated, while the concave diffusion term is explicitly computed by a second order extrapolation, which comes from the second order convex splitting idea. In addition, a second-order Douglas-Dupont regularization, in the the form of $A\tau\Delta(\phi_i^{n+1}-\phi_i^n)$, is employed in the numerical algorithm, to achieve a modified energy stability; see similar techniques reported in [17].

This paper is organized as follows. In Section 2, we propose the numerical scheme using the mass lumped finite element method. The positivity-preserving property of the numerical solution and the energy stability analysis are established in Section 3. In Section 4, the numerical simulations are presented to verify the theoretical results. Finally, some concluding remarks are given in Section 5.

2 Preliminary notations and the fully discrete scheme

Consider standard notation of the Sobolev spaces $W^{m,p}(\Omega)$ with $\|\cdot\|_{m,p}$, and $\|\cdot\|_{0,p}=\|\cdot\|_p$, $\|\cdot\|_{0,2}=\|\cdot\|_2=\|\cdot\|$, and $\|\cdot\|_{q,2}=\|\cdot\|_{H^q}$. Let $C^\infty_{per}(\Omega)$ be the set of all restrictions onto Ω of all real-valued, L-periodic, $C^\infty(\Omega)$-functions on $\mathbb{R}^2$. For each integer $q\geq 0$, denote $H^q_{per}(\Omega)$ as the closure of $C^\infty_{per}(\Omega)$ in the usual Sobolev norm $\|\cdot\|_q$, and $H^{-q}_{per}(\Omega)$ be the dual space of $H^q_{per}(\Omega)$. It is clear that $H^0_{per}(\Omega)=L^2(\Omega)$, and we denote $\frac{\delta F}{\delta\phi_1}=\delta_{\phi_1}F$, $\frac{\delta F}{\delta\phi_2}=\delta_{\phi_2}F$. In turn, the mixed weak formulation of the ternary MMC-TDGL equations (1.2) becomes: find $\phi_1,\mu_1,\phi_2,\mu_2\in L^2(0,T;H^1_{per}(\Omega))$, with $\partial_t\phi_1$, $\partial_t\phi_2\in L^2(0,T;H^{-1}_{per}(\Omega))$, satisfying

$$\begin{cases}(\partial_t\phi_1,v_1)+(D_1\nabla\mu_1,\nabla v_1)=0, & \forall v_1\in H^1_{per}(\Omega),\\ (\mu_1,w_1)=\left(\delta_{\phi_1}F\left(\phi_1,\phi_2\right),w_1\right), & \forall w_1\in H^1_{per}(\Omega),\\ (\partial_t\phi_2,v_2)+(D_2\nabla\mu_2,\nabla v_2)=0, & \forall v_2\in H^1_{per}(\Omega),\\ (\mu_2,w_2)=\left(\delta_{\phi_2}F\left(\phi_1,\phi_2\right),w_2\right), & \forall w_2\in H^1_{per}(\Omega),\end{cases} \tag{2.1}$$

for any $t \in [0,T]$, where $(\cdot,\cdot)$ represents the L^2 inner product or the duality pairing.

2.1 The mass lumped finite element approximation

Let $\mathcal{T}_h$ be a shape-regular triangulation of Ω, with mesh size h, and denote h_e as the diameter of each triangle $e \in \mathcal{T}_h$ and $\triangle_e$ the area of e. Of course, the element is shape regular, and we assume that $\frac{h_e^2}{\triangle_e}$ is uniformly bounded by a given constant: $\frac{h_e^2}{\triangle_e} \le C_{\mathcal{T}}$. Based on the quasi-uniform triangulated mesh $\mathcal{T}_h$, the finite element space is introduced as

$$S_h := \{v \in H^1_{per}(\Omega) \mid \ v \text{ is piecewise linear on each } e \in \mathcal{T}_h\} = \text{span}\{\chi_j \mid j = 1, \cdots, N_p\},$$

where $\chi_j \in S_h$ is the j^{th} Lagrange nodal basis function, with the property $\chi_j(P_i) = \delta_{i,j}$. Define $\mathring{S}_h := S_h \cap L_0^2(\Omega)$, with $L_0^2(\Omega) = \{v \in L^2(\Omega) \mid (v,1) = 0\}$, the function space with zero mean in $L^2(\Omega)$.

The standard mixed finite element method (FEM) faces theoretical difficulties in ensuring the positivity-preserving property. To tackle this subtle challenge, we choose to employ the mass-lumped FEM, which represents an enhancement of the standard FEM for solving parabolic equations. It simplifies the computation for the inverse of mass matrix and overcomes the shortage of the standard FEM that can not preserve the maximum principle for homogeneous parabolic equations. In more details, let $P_{e,k}(k = 1, 2, 3)$ be the three vertices of triangle e. The generation of the mass lumped matrix can be regarded as introducing the following quadrature formula:

$$Q_h(f) = \sum_{e \in \mathcal{T}_h} Q_e(f), \quad \forall f \in C(\Omega; \mathbb{R}),$$

where

$$Q_e(f) = \frac{\triangle_e}{3} \sum_{k=1}^{3} f\left(P_{e,k}\right) \approx \int_e f d\mathbf{x}.$$

By the above quadrature formula, it is easy to derive $Q_h(\chi_j \chi_k) = 0$ for $k \neq j$, so that

$$Q_h(\chi_j \chi_k) = \delta_{j,k} Q_h(\chi_j^2), \quad j, k = 1, \cdots, N_p.$$

It is obvious that

$$Q_h(\chi_j^2) = \sum_{e \in \mathcal{T}_h} Q_e\left(\chi_j^2\right) = \frac{1}{3} \text{area}\left(D_j\right), \quad D_j := \text{supp}(\chi_j).$$

We define an approximation of the canonical inner product on S_h by

$$(\psi, \eta)_Q := Q_h(\psi\eta), \quad \forall \psi, \eta \in S_h.$$

Next, we define a norm $\|\eta\|_Q := \sqrt{(\eta,\eta)_Q}$ for any $\eta \in S_h$. This norm is observed to be equivalent to the standard $\|\cdot\|_{L^2}$ norm by considering each triangle separately.

For the convenience of the theoretical analysis, we have to modify the definition of the discrete Laplacian operator and the discrete H^{-1} norm. The primary difference is associated with the integral definition.

Definition 2.1. *The discrete Laplacian operator $\Delta_h : S_h \to \mathring{S}_h$ is defined as follows: for any $v_h \in S_h, \Delta_h v_h \in \mathring{S}_h$ denote the unique solution to the problem*

$$(\Delta_h v_h, \chi)_Q = -(\nabla v_h, \nabla \chi), \quad \forall \chi \in S_h.$$

It is straightforward to verify that by restricting the domain, $\Delta_h : \mathring{S}_h \to \mathring{S}_h$ beccomes invertible, and for any $v_h \in \mathring{S}_h$, we see that

$$\left(\nabla (-\Delta_h)^{-1} v_h, \nabla \chi\right) = (v_h, \chi)_Q, \quad \forall \chi \in S_h.$$

Definition 2.2. *The discrete H^{-1} norm $\|\cdot\|_{-1,Q}$, is defined as follows:*

$$\|v_h\|_{-1,Q} := \sqrt{(v_h, (-\Delta_h)^{-1} v_h)_Q}, \quad \forall v_h \in \mathring{S}_h.$$

2.2 Convex-concave decomposition

The existence of the convex-concave decomposition of the energy functional $F(\phi_1, \phi_2)$ in (1.1) has been derived in [14], i.e, $F(\phi_1, \phi_2)$ admits a (not necessarily unique) splitting into purely convex and concave parts, $F = F_c - F_e$, where $F_c = \int_\Omega S(\phi_1, \phi_2) + K(\phi_1, \phi_2)\, d\mathbf{x}$ and $F_e = -\int_\Omega H(\phi_1, \phi_2)\, d\mathbf{x}$ are convex with respect to the specific variables, provided that $4\chi_{13}\chi_{23} - (\chi_{12} - \chi_{13} - \chi_{23})^2 > 0$.

Definition 2.3. *Define the discrete energy $\hat{E} : S_h \times S_h \to \mathbb{R}$ as follows*

$$\hat{E}(\phi_1, \phi_2) = (S(\phi_1, \phi_2), 1)_Q + (H(\phi_1, \phi_2), 1)_Q + (\tilde{K}(\phi_1, \phi_2), 1),$$

where

$$\tilde{K}(\phi_1, \phi_2) := \sum_{\ell=1}^{3} \frac{a_\ell^2 |\nabla \phi_\ell|^2}{36 \mathcal{A}(\phi_\ell)},$$

and the operator $\mathcal{A}$ represents element average operator, that is,

$$\mathcal{A}(\phi)|_e := \frac{1}{3}(\phi_\alpha + \phi_\beta + \phi_\gamma) = \frac{1}{\triangle_e} \int_e \phi d\mathbf{x}, \quad \forall \phi \in S_h.$$

Notice that ϕ_α, ϕ_β, and ϕ_γ represent the values of ϕ at the three vertices of the element e.

The following lemma states the existence of a convex-concave decomposition, and its proof is similar to that in [14, 44]; the technical details are skipped for the sake of brevity.

Lemma 2.1. *[44] Suppose $\phi_1, \phi_2 \in S_h$, if $4\chi_{13}\chi_{23} - (\chi_{12} - \chi_{13} - \chi_{23})^2 > 0$, the functions*

$$\hat{E}_c = (S(\phi_1, \phi_2), 1)_Q + (\tilde{K}(\phi_1, \phi_2), 1), \tag{2.2}$$

$$\hat{E}_e = (-H(\phi_1, \phi_2), 1)_Q, \tag{2.3}$$

are convex. As a result, $\hat{E}(\phi_1, \phi_2) = \hat{E}_c(\phi_1, \phi_2) - \hat{E}_e(\phi_1, \phi_2)$ is a convex-concave decomposition of the discrete energy.

In addition, the following lemma is needed for the later analysis.

Lemma 2.2. *[44] Suppose that $\Omega = (0, L)^2$ and $\phi_1, \phi_2, \psi_1, \psi_2 : \Omega \to \mathbb{R}$ are periodic and sufficiently regular. Consider the convex-concave decomposition of the energy $\hat{E}(\phi_1, \phi_2)$ into $\hat{E} = \hat{E}_c - \hat{E}_e$, given by (2.2)-(2.3), then we have*

$$\begin{aligned}\hat{E}(\phi_1, \phi_2) - \hat{E}(\psi_1, \psi_2) \le & \left(\frac{\partial}{\partial \phi_1} S(\phi_1, \phi_2) + \frac{\partial}{\partial \phi_1} H(\psi_1, \psi_2), \phi_1 - \psi_1 \right)_Q + (\delta_{\phi_1} \tilde{K}(\phi_1, \phi_2), \phi_1 - \psi_1) \\ & + \left(\frac{\partial}{\partial \phi_2} S(\phi_1, \phi_2) + \frac{\partial}{\partial \phi_2} H(\psi_1, \psi_2), \phi_2 - \psi_2 \right)_Q + (\delta_{\phi_2} \tilde{K}(\phi_1, \phi_2), \phi_2 - \psi_2).\end{aligned}$$

2.3 The fully discrete numerical scheme

The fully-discrete scheme is constructed in this section. Denote a positive integer M as the total number of time steps, and let $0 = t_0 < t_1 < \cdots < t_M = M\tau = T$ be a uniform partition of $[0, T]$, with $\tau = t_i - t_{i-1}$ and $i = 1, \cdots, M$. The convex-concave decomposition $\hat{E} = \hat{E}_c - \hat{E}_e$ implies that the potentials could also be split into two parts, namely μ_1 and μ_2. With an implicit treatment for the convex term and an explicit computation of the concave, the second-order mass lumped finite element scheme is proposed as follows: $\forall v_1, v_2, w_1, w_2 \in S_h$, find $\phi_{1h}^{n+1}, \mu_{1h}^{n+1}, \phi_{2h}^{n+1}, \mu_{2h}^{n+1} \in S_h$ such that

$$\left(\frac{\frac{3}{2}\phi_{1h}^{n+1} - 2\phi_{1h}^{n} + \frac{1}{2}\phi_{1h}^{n-1}}{\tau}, v_1 \right)_Q = -\left(D_1 \nabla \mu_{1h}^{n+1}, \nabla v_1 \right), \tag{2.4a}$$

$$\begin{aligned}\left(\mu_{1h}^{n+1}, w_1 \right)_Q = & \left(\delta_{\phi_1} S\left(\phi_{1h}^{n+1}, \phi_{2h}^{n+1} \right), w_1 \right)_Q + \left(\delta_{\phi_1} \tilde{K}\left(\phi_{1h}^{n+1}, \phi_{2h}^{n+1} \right), w_1 \right) \\ & + \left(\delta_{\phi_1} H\left(\check{\phi}_{1h}^{n+1}, \check{\phi}_{2h}^{n+1} \right), w_1 \right)_Q + A\tau(\nabla(\phi_{1h}^{n+1} - \phi_{1h}^{n}), \nabla w_1),\end{aligned} \tag{2.4b}$$

$$\left(\frac{\frac{3}{2}\phi_{2h}^{n+1} - 2\phi_{2h}^{n} + \frac{1}{2}\phi_{2h}^{n-1}}{\tau}, v_2 \right)_Q = -\left(D_2 \nabla \mu_{2h}^{n+1}, \nabla v_2 \right), \tag{2.4c}$$

$$\begin{aligned}\left(\mu_{2h}^{n+1}, w_2 \right)_Q = & \left(\delta_{\phi_2} S\left(\phi_{1h}^{n+1}, \phi_{2h}^{n+1} \right), w_2 \right)_Q + \left(\delta_{\phi_2} \tilde{K}\left(\phi_{1h}^{n+1}, \phi_{2h}^{n+1} \right), w_2 \right) \\ & + \left(\delta_{\phi_2} H\left(\check{\phi}_{1h}^{n+1}, \check{\phi}_{2h}^{n+1} \right), w_2 \right)_Q + A\tau(\nabla(\phi_{2h}^{n+1} - \phi_{2h}^{n}), \nabla w_2),\end{aligned} \tag{2.4d}$$

where $\check{\phi}_h^{n+1} = 2\phi_h^n - \phi_h^{n-1}$ and for $i = 1, 2$,

$$\begin{aligned}\left(\delta_{\phi_i} \tilde{K}(\phi_1, \phi_2), w_i \right) = & \left(-\frac{a_i^2 |\nabla \phi_i|^2}{36(\mathcal{A}(\phi_i))^2}, w_i \right) + \left(\frac{a_i^2 \nabla \phi_i}{18\mathcal{A}(\phi_i)}, \nabla w_i \right) \\ & + \left(\frac{a_3^2 |\nabla (1 - \phi_1 - \phi_2)|^2}{36 (1 - \mathcal{A}(\phi_1) - \mathcal{A}(\phi_2))^2}, w_i \right) - \left(\frac{a_3^2 \nabla (1 - \phi_1 - \phi_2)}{18 (1 - \mathcal{A}(\phi_1) - \mathcal{A}(\phi_2))}, \nabla w_i \right).\end{aligned}$$

Notice that a second-order Adams-Bashforth explicit extrapolation formula and an artificial Douglas-Dupont regularization terms have been added, where the artificial terms aim to ensure the energy dissipation.

3 Numerical analysis

3.1 Unique solvability and positivity-preserving property

The mass lumped spatial approximation improves the original mass matrix, and this improvement leads to an efficient approach to theoretically justify the preserving positivity property for the ternary MMC system.

The following results in [44, 45] are needed in the theoretical proof.

Lemma 3.1. *Suppose that $\xi, \bar{\xi} \in S_h$, with $(\xi - \bar{\xi}, 1) = 0$, that is, $\xi - \bar{\xi} \in \mathring{S}_h$, and assume that $\|\xi\|_\infty < 1, \|\bar{\xi}\|_\infty \le M$. Then, we have the following estimate:*

$$\left\| -\Delta_h^{-1} \left(\xi - \bar{\xi} \right) \right\|_\infty \le C_1,$$

where $C_1 > 0$ depends only upon M and Ω. In particular, C_1 is independent of the mesh spacing h.

Lemma 3.2. *For any $\phi \in S_h$, if $\mathcal{A}(\phi) > 0$ on one element $e \in \mathcal{T}_h$ with mesh size h_e, by careful calculation, we have*

$$\frac{|\nabla \phi|}{\mathcal{A}(\phi)} \le \frac{3\sqrt{2} h_e}{2 \triangle_e}$$

on the element e.

Lemma 3.3. *Let $\phi, \psi \in S_h$ and $\mathcal{A}(\psi) > 0$, then*

$$\left(-\frac{|\nabla \phi|^2}{36 (\mathcal{A}(\phi))^2}, \psi \right) + \left(\frac{\nabla \phi}{18 \mathcal{A}(\phi)}, \nabla \psi \right) \le \frac{1}{36} \left(\frac{\nabla \psi}{\mathcal{A}(\psi)}, \nabla \psi \right) \le \frac{C_{\mathcal{T}}}{8} \sum_{e \in \mathcal{T}_h} \mathcal{A}(\psi)|_e,$$

$$\left(\frac{|\nabla \phi|^2}{36 (\mathcal{A}(\phi))^2}, \psi \right) - \left(\frac{\nabla \phi}{18 \mathcal{A}(\phi)}, \nabla \psi \right) \le \left(\frac{|\nabla \phi|^2}{18 (\mathcal{A}(\phi))^2}, \mathcal{A}(\psi) \right) + \frac{1}{36} \left(\frac{\nabla \psi}{\mathcal{A}(\psi)}, \nabla \psi \right) \le \frac{3 C_{\mathcal{T}}}{8} \sum_{e \in \mathcal{T}_h} \mathcal{A}(\psi)|_e.$$

Remark 3.1. *In the case of $\mathcal{A}(\psi) \ge 0$, the inequalities in Lemma 3.3 could be modified as*

$$\left(-\frac{|\nabla \phi|^2}{36 (\mathcal{A}(\phi))^2}, \psi \right) + \left(\frac{\nabla \phi}{18 \mathcal{A}(\phi)}, \nabla \psi \right) \le \frac{1}{36} \sum_{\substack{e \in \mathcal{T}_h \\ \mathcal{A}(\psi) > 0}} \left(\frac{\nabla \psi}{\mathcal{A}(\psi)}, \nabla \psi \right)_e,$$

$$\left(\frac{|\nabla \phi|^2}{36 (\mathcal{A}(\phi))^2}, \psi \right) - \left(\frac{\nabla \phi}{18 \mathcal{A}(\phi)}, \nabla \psi \right) \le \left(\frac{|\nabla \phi|^2}{18 (\mathcal{A}(\phi))^2}, \mathcal{A}(\psi) \right) + \frac{1}{36} \sum_{\substack{e \in \mathcal{T}_h \\ \mathcal{A}(\psi) > 0}} \left(\frac{\nabla \psi}{\mathcal{A}(\psi)}, \nabla \psi \right)_e.$$

Lemma 3.4. *For any $\phi \in S_h$, if χ_j is piecewise linear basis function, then we have*

$$(\nabla \phi, \nabla \chi_j) \le \sum_{e \in D_j} \frac{h_e^2}{2 \triangle_e} \sum_{i=1}^{3} \phi(P_{e,i})$$

on $\mathcal{T}_h$ with mesh size h_e.

The unique solvability and positivity-preserving property is stated in the following theorem.

Theorem 3.1. *Given $\phi_1^k, \phi_2^k \in S_h$, with $0 < \phi_1^k, \phi_2^k < 1$, $0 < \phi_1^k + \phi_2^k < 1$, $k = n-1, n$, $\overline{\phi_1^n} = \overline{\phi_1^{n-1}}$, $\overline{\phi_2^n} = \overline{\phi_2^{n-1}}$, there exists a unique solution $\phi_1^{n+1}, \phi_2^{n+1} \in S_h$ to (2.4), with $\overline{\phi_1^{n+1}} = \overline{\phi_1^n}$, $\overline{\phi_2^{n+1}} = \overline{\phi_2^n}$, $0 < \phi_1^{n+1}, \phi_2^{n+1} < 1$, and $0 < \phi_1^{n+1} + \phi_2^{n+1} < 1$.*

Proof. A careful calculation reveals that, the numerical solution turns out to a minimizer of the following discrete energy functional with respect to ϕ_1 and ϕ_2:

$$\begin{aligned}
\mathcal{J}^n (\phi_1, \phi_2) =& \frac{1}{3 D_1 \tau} \left\| \frac{3}{2} \phi_1 - 2 \phi_1^n + \frac{1}{2} \phi_1^{n-1} \right\|_{-1,Q}^2 + \frac{1}{3 D_2 \tau} \left\| \frac{3}{2} \phi_2 - 2 \phi_2^n + \frac{1}{2} \phi_2^{n-1} \right\|_{-1,Q}^2 \\
& + \left(S (\phi_1, \phi_2), 1 \right)_Q + \left(\tilde{K} (\phi_1, \phi_2), 1 \right) \\
& + \left(\delta_{\phi_1} H \left(\check{\phi}_1^{n+1}, \check{\phi}_2^{n+1} \right), \phi_1 \right)_Q + \left(\delta_{\phi_2} H \left(\check{\phi}_1^{n+1}, \check{\phi}_2^{n+1} \right), \phi_2 \right)_Q \\
& + \frac{A\tau}{2} \|\nabla \phi_1\|^2 + \frac{A\tau}{2} \|\nabla \phi_2\|^2 - (\nabla \phi_1, A\tau \nabla \phi_1^n) - (\nabla \phi_2, A\tau \nabla \phi_2^n)
\end{aligned}$$

over the admissible set

$$A_h := \{(\phi_1, \phi_2) \in S_h \times S_h \mid 0 \le \phi_1, \phi_2 \le 1, 0 \le \phi_1 + \phi_2 \le 1, \\ \left(\phi_1 - \overline{\phi_1^0}, 1\right)_Q = 0, \quad \left(\phi_2 - \overline{\phi_2^0}, 1\right)_Q = 0\}.$$

Meanwhile, it is straightforward to verify that $\mathcal{J}^n$ is a strictly convex functional with respect to ϕ_1 and ϕ_2 over A_h. To facilitate the later analysis, the following closed domain is taken into consideration:

$$A_{h,\delta} := \{(\phi_1, \phi_2) \in S_h \times S_h \mid \phi_1, \phi_2 \ge g(\delta), \delta \le \phi_1 + \phi_2 \le 1 - \delta, \\ \left(\phi_1 - \overline{\phi_1^0}, 1\right)_Q = 0, \left(\phi_2 - \overline{\phi_2^0}, 1\right)_Q = 0\}.$$

Of course, $A_{h,\delta}$ is a bounded, compact and convex set in the following hyperplane V:

$$V = \left\{(\phi_1, \phi_2) : \frac{1}{|\Omega|}(\phi_1, 1)_Q = \overline{\phi_1^0}, \ \ \frac{1}{|\Omega|}(\phi_2, 1)_Q = \overline{\phi_2^0}\right\}.$$

As a result, there exists a minimizer of $\mathcal{J}^n(\phi_1, \phi_2)$ over $A_{h,\delta}$ (may not be unique, and the uniqueness argument will be provided later). The key point of the theoretical analysis is that, such a minimizer could not occur on the functional boundary points if δ and $g(\delta)$ are small enough.

Using proof by contradiction, assume the minimizer of $\mathcal{J}^n(\phi_1, \phi_2)$ occurs at a functional boundary point of $A_{h,\delta}$. We will complete the proof by considering four distinct cases. To avoid redundancy, we focus on analyzing two representative cases; the details are provided below.
Case 1: The minimization point is given by $(\phi_1^\star, \phi_2^\star)$, with $\phi_1^\star(P_{\alpha_0}) := \phi_{1,\alpha_0}^\star = g(\delta)$. Meanwhile, it is assumed that $\phi_1^\star$ reaches the maximum value at α_1, so that we have $\phi_{1,\alpha_1}^\star \ge \overline{\phi_1^\star} = \overline{\phi_1^0}$. Of course, the variable ϕ_{1,α_1} could be represented as the N_p-th one in the hyperplane V, with the constraint

$$\phi_{1,\alpha_1} = \frac{(\overline{\phi_1^0}, 1)_Q - \sum_{i \ne \alpha_1}^{N_p} (\phi_{1,i}, \chi_i)_Q}{(\chi_{\alpha_1}, 1)_Q}.$$

A detailed calculation gives the following directional derivative

$$\begin{aligned} d_s \mathcal{J}^n\left(\phi_1^\star + s\psi, \phi_2^\star\right)|_{s=0} =& \frac{1}{D_1 \tau}\left(-\Delta_h^{-1}\left(\frac{3}{2}\phi_1^\star - 2\phi_1^n + \frac{1}{2}\phi_1^{n-1}\right), \psi\right)_Q + \left(\delta_{\phi_1} S\left(\phi_1^\star, \phi_2^\star\right), \psi\right)_Q \\ &+ \left(\delta_{\phi_1} \tilde{K}\left(\phi_1^\star, \phi_2^\star\right), \psi\right) + \left(\delta_{\phi_1} H\left(\check{\phi}_1^{n+1}, \check{\phi}_2^{n+1}\right), \psi\right)_Q + A\tau(\nabla(\phi_1^\star - \phi_1^n), \nabla\psi), \end{aligned} \tag{3.1}$$

for any $\psi \in S_h$, $(\phi_1^\star + s\psi, \phi_2^\star) \in A_{h,\delta}$. In turn, we pick the direction

$$\psi = \delta_{\alpha_0} - C_2 \delta_{\alpha_1} \in S_h, \quad C_2 = \frac{\text{area}(D_{\alpha_0})}{\text{area}(D_{\alpha_1})},$$

in which δ_{α_0} and δ_{α_1} are the basis functions on P_{α_0} and P_{α_1}, D_{α_0} and D_{α_1} are the support of δ_{α_0} and δ_{α_1}, respectively.

An application of Lemma 3.1 gives a bound for the first term appearing in (3.1):

$$
\begin{aligned}
&\frac{1}{D_1\tau}(-\Delta_h^{-1}(\frac{3}{2}\phi_1^\star-2\phi_1^n+\frac{1}{2}\phi_1^{n-1}),\psi)_Q\\
=&\frac{1}{D_1\tau}\sum_{e\in\mathcal{T}_h}\frac{\triangle_e}{3}\sum_{j=1}^{3}(-\Delta_h^{-1})(\frac{3}{2}\phi_1^\star-2\phi_1^n+\frac{1}{2}\phi_1^{n-1})\psi(P_{e,j})\\
=&\frac{1}{3D_1\tau}\left(\operatorname{area}(D_{\alpha_0})(-\Delta_h^{-1})(\frac{3}{2}\phi_1^\star-2\phi_1^n+\frac{1}{2}\phi_1^{n-1})|_{\alpha_0}\right.\\
&\left.-C_2\operatorname{area}(D_{\alpha_1})(-\Delta_h^{-1})(\frac{3}{2}\phi_1^\star-2\phi_1^n+\frac{1}{2}\phi_1^{n-1})|_{\alpha_1}\right)\\
=&\frac{1}{3D_1\tau}\operatorname{area}(D_{\alpha_0})\left((-\Delta_h^{-1})(\frac{3}{2}\phi_1^\star-2\phi_1^n+\frac{1}{2}\phi_1^{n-1})|_{\alpha_0}\right.\\
&\left.-(-\Delta_h^{-1})(\frac{3}{2}\phi_1^\star-2\phi_1^n+\frac{1}{2}\phi_1^{n-1})|_{\alpha_1}\right)\\
\le&\frac{4C_1}{3D_1\tau}\operatorname{area}(D_{\alpha_0}).
\end{aligned}
\tag{3.2}
$$

The second term could be analyzed as follows:

$$
\begin{aligned}
(\delta_{\phi_1}S(\phi_1^\star,\phi_2^\star),\psi)_Q=&\left(\frac{1}{\gamma}\ln(\frac{\alpha\phi_1^\star}{\gamma})-\ln(1-\phi_1^\star-\phi_2^\star),\psi\right)_Q\\
=&\sum_{e\in\mathcal{T}_h}\left(\frac{1}{3}\triangle_e\sum_{j=1}^{3}\left(\frac{1}{\gamma}\ln(\frac{\alpha\phi_1^\star}{\gamma})-\ln(1-\phi_1^\star-\phi_2^\star)\right)\psi(P_{e,j})\right)\\
=&\frac{1}{3}\operatorname{area}(D_{\alpha_0})\left(\left(\frac{1}{\gamma}\ln(\frac{\alpha\phi_1^\star}{\gamma})-\ln(1-\phi_1^\star-\phi_2^\star)\right)|_{\alpha_0}\right.\\
&\left.-\left(\frac{1}{\gamma}\ln(\frac{\alpha\phi_1^\star}{\gamma})-\ln(1-\phi_1^\star-\phi_2^\star)\right)|_{\alpha_1}\right)\\
=&\frac{1}{3}\operatorname{area}(D_{\alpha_0})\left(\ln\frac{(\phi_1^\star)^{\frac{1}{\gamma}}}{1-\phi_1^\star-\phi_2^\star}|_{\alpha_0}-\ln\frac{(\phi_1^\star)^{\frac{1}{\gamma}}}{1-\phi_1^\star-\phi_2^\star}|_{\alpha_1}\right)\\
\le&\frac{1}{3}\operatorname{area}(D_{\alpha_0})\Big(\ln\frac{(g(\delta))^{\frac{1}{\gamma}}}{\delta}-\ln\frac{(\overline{\phi_1^0})^{\frac{1}{\gamma}}}{1-\delta}\Big)\\
\le&\frac{1}{3}\operatorname{area}(D_{\alpha_0})\Big(\ln\frac{(g(\delta))^{\frac{1}{\gamma}}}{\delta}-\ln(\overline{\phi_1^0})^{\frac{1}{\gamma}}\Big).
\end{aligned}
\tag{3.3}
$$

A decomposition for the third term is straightforward:

$$
\begin{aligned}
&\left(\delta_{\phi_1}\tilde{K}\left(\phi_1^\star,\phi_2^\star\right),\psi\right)\\
=&\left(-\frac{a_1^2|\nabla\phi_1^\star|^2}{36(\mathcal{A}(\phi_1^\star))^2},\psi\right)+\left(\frac{a_1^2\nabla\phi_1^\star}{18\mathcal{A}(\phi_1^\star)},\nabla\psi\right)\\
&+\left(\frac{a_3^2\left|\nabla\left(1-\phi_1^\star-\phi_2^\star\right)\right|^2}{36\left(\mathcal{A}(1-\phi_1^\star-\phi_2^\star)\right)^2},\psi\right)-\left(\frac{a_3^2\nabla\left(1-\phi_1^\star-\phi_2^\star\right)}{18\mathcal{A}\left(1-\phi_1^\star-\phi_2^\star\right)},\nabla\psi\right).
\end{aligned}
\tag{3.4}
$$

With the help of Lemma 3.3, the following bounds are available:

$$\begin{aligned}&\left(-\frac{a_1^2|\nabla\phi_1^\star|^2}{36(\mathcal{A}(\phi_1^\star))^2},\psi\right)+\left(\frac{a_1^2\nabla\phi_1^\star}{18\mathcal{A}(\phi_1^\star)},\nabla\psi\right)\\ \le&\frac{a_1^2C_{\mathcal{T}}}{8}\sum_{e\in\mathcal{T}_h}\mathcal{A}(\delta_{\alpha_0})|_e+\frac{3a_1^2C_2C_{\mathcal{T}}}{8}\sum_{e\in\mathcal{T}_h}\mathcal{A}(\delta_{\alpha_1})|_e=\frac{a_1^2C_{\mathcal{T}}}{24}\sum_{e\in D_{\alpha_0}}1+\frac{a_1^2C_2C_{\mathcal{T}}}{8}\sum_{e\in D_{\alpha_1}}1,\end{aligned}\tag{3.5}$$

$$\left(\frac{a_3^2\left|\nabla\left(1-\phi_1^\star-\phi_2^\star\right)\right|^2}{36\left(\mathcal{A}(1-\phi_1^\star-\phi_2^\star)\right)^2},\psi\right)-\left(\frac{a_3^2\nabla\left(1-\phi_1^\star-\phi_2^\star\right)}{18\mathcal{A}\left(1-\phi_1^\star-\phi_2^\star\right)},\nabla\psi\right)\le\frac{a_3^2C_{\mathcal{T}}}{8}\sum_{e\in D_{\alpha_0}}1+\frac{a_3^2C_2C_{\mathcal{T}}}{24}\sum_{e\in D_{\alpha_1}}1.\tag{3.6}$$

Subsequently, an estimate for the term $\delta_{\phi_1}\tilde{K}$ becomes a direct consequence:

$$\left(\delta_{\phi_1}\tilde{K}\left(\phi_1^\star,\phi_2^\star\right),\psi\right)\le\frac{(3a_1^2+a_3^2)C_{\mathcal{T}}}{24}\sum_{e\in D_{\alpha_0}}1+\frac{(a_1^2+3a_3^2)C_2C_{\mathcal{T}}}{24}\sum_{e\in D_{\alpha_1}}1.\tag{3.7}$$

In terms of the numerical solution ϕ_1^k, $k=n-1,n$, at the previous time steps, the a-priori assumption $0<\phi_1^k<1$ yields the following bound:

$$-3\le\check{\phi}_1^{n+1}(P_{\alpha_0})-\check{\phi}_1^{n+1}(P_{\alpha_1})\le 3.$$

Regarding the concave part, we see that

$$\begin{aligned}&\left(\delta_{\phi_1}H\left(\check{\phi}_1^{n+1},\check{\phi}_2^{n+1}\right),\psi\right)_Q\\ =&(\chi_{13}-2\chi_{13}\check{\phi}_1^{n+1}+(\chi_{12}-\chi_{13}-\chi_{23})\check{\phi}_2^{n+1},\psi)_Q\\ =&\sum_{e\in\mathcal{T}_h}\frac{1}{3}\triangle_e\left(\sum_{j=1}^{3}(\chi_{13}-2\chi_{13}\check{\phi}_1^{n+1}-(\chi_{12}-\chi_{13}-\chi_{23})\check{\phi}_2^{n+1})\psi(P_{e,j})\right)\\ =&\frac{1}{3}\operatorname{area}(D_{\alpha_0})\left(-2\chi_{13}(\check{\phi}_1^{n+1}|_{\alpha_0}-\check{\phi}_1^{n+1}|_{\alpha_1})-(\chi_{12}-\chi_{13}-\chi_{23})(\check{\phi}_2^{n+1}|_{\alpha_0}-\check{\phi}_2^{n+1}|_{\alpha_1})\right)\\ \le&\operatorname{area}(D_{\alpha_0})(\chi_{12}+3\chi_{13}+\chi_{23}).\end{aligned}\tag{3.8}$$

Meanwhile, the artificial regularization term could be analyzed as follows, with the help of Lemma 3.4:

$$\begin{aligned}&A\tau(\nabla(\phi_1^\star-\phi_1^n),\nabla\psi)\\ =&A\tau(\nabla(\phi_1^\star-\phi_1^n),\nabla\delta_{\alpha_0})-A\tau C_2(\nabla(\phi_1^\star-\phi_1^n),\nabla\delta_{\alpha_1})\\ =&-A\tau(\nabla\phi_1^n,\nabla\delta_{\alpha_0})+A\tau C_2(\nabla\phi_1^n,\nabla\delta_{\alpha_1})\\ \le&A\tau\left(\sum_{e\in D_{\alpha_0}}\frac{h_e^2}{2\triangle_e}\sum_{i=1}^{3}\phi_1^n(P_{e,i})+C_2\sum_{e\in D_{\alpha_1}}\frac{h_e^2}{2\triangle_e}\sum_{i=1}^{3}\phi_1^n(P_{e,i})\right)\\ \le&6C_{\mathcal{T}}A\tau\operatorname{area}(D_{\alpha_0}).\end{aligned}\tag{3.9}$$

In turn, a substitution of the above estimates (3.2)-(3.9) into (3.1) leads to

$$d_s\mathcal{J}^n\left(\phi_1^\star+s\psi,\phi_2^\star\right)|_{s=0}\le\frac{1}{3}\operatorname{area}(D_{\alpha_0})\ln\frac{(g(\delta))^{\frac{1}{\gamma}}}{\delta}+r_0,$$

with $r_0 = \text{area}(D_{\alpha_0})(\frac{4C_1}{3D_1\tau} - \ln(\overline{\phi_1^0})^{\frac{1}{\gamma}} + \chi_{12} + 3\chi_{13} + \chi_{23} + 6C_{\mathcal{T}}A\tau) + \frac{(3a_1^2+a_3^2)C_{\mathcal{T}}}{24}\sum_{e\in D_{\alpha_0}} 1 + \frac{(a_1^2+3a_3^2)C_2C_{\mathcal{T}}}{24}\sum_{e\in D_{\alpha_1}} 1$. It is clear that r_0 is a constant for fixed τ, h, while it becomes singular as $\tau \to 0$. For a fixed τ, $g(\delta)$ could be chosen sufficiently small so that

$$\frac{1}{3}\,\text{area}(D_{\alpha_0})\ln\frac{(g(\delta))^{\frac{1}{\gamma}}}{\delta} + r_0 < 0. \tag{3.10}$$

In fact, one typical choice is given by $g(\delta) = \left(\delta \exp\left(-\frac{3(r_0+1)}{\text{area}(D_{\alpha_0})}\right)\right)^{\gamma}$. As a result, the following inequality is valid:

$$d_{\text{s}}\mathcal{J}^n\left(\phi_1^\star + s\psi, \phi_2^\star\right)|_{s=0} < 0.$$

This inequality contradicts the assumption that $\mathcal{J}^n$ has a minimum at $(\phi_1^\star, \phi_2^\star)$, since the directional derivative is negative in a direction pointing into $(A_{h,\delta})^\circ$, the interior of $A_{h,\delta}$.

Case 2: The global minimum of $\mathcal{J}^n$ over $A_{h,\delta}$ could not occur on the functional boundary section of $\phi_{2,\alpha_0} = g(\delta)$, for any grid node number α_0, if $g(\delta)$ is small enough. This fact could be proved using similar arguments as in Case 1, and the technical details are left to interested readers.

Case 3: The minimization point is given by $(\phi_1^\star, \phi_2^\star)$, with $\phi_{1,\alpha_0}^\star + \phi_{2,\alpha_0}^\star = 1 - \delta$, and α_0 is the α_0-th grid node number. Without loss of generality, we assume that $\phi_{1,\alpha_0} \geq \frac{1}{3}$. Meanwhile, by the fact that $(\phi_1 + \phi_2, 1) = \overline{\phi_1^0} + \overline{\phi_2^0}$, there exists one grid point $\alpha_1 = (i_1, j_1)$, so that $\phi_1^\star + \phi_2^\star$ reaches the maximum value. Of course, an obvious bound becomes available: $\phi_{1,\alpha_1}^\star + \phi_{2,\alpha_1}^\star \leq \overline{\phi_1^\star} + \overline{\phi_2^\star} = \overline{\phi_1^0} + \overline{\phi_2^0}$. Using similar arguments, the variable ϕ_{1,α_1} could be rewritten as the N_p-th one in the hyperplane V, with the constraint

$$\phi_{1,\alpha_1} = \frac{(\overline{\phi_1^0}, 1)_Q - \sum_{i\neq\alpha_1}^{N_p}(\phi_{1,i}, \chi_i)_Q}{(\chi_{\alpha_1}, 1)_Q}.$$

In this case, a careful calculation yields the corresponding directional derivative

$$\begin{aligned}
&d_s\mathcal{J}^n\left(\phi_1^\star + s\psi, \phi_2^\star\right)|_{s=0} \\
=&\frac{1}{D_1\tau}\left(-\Delta_h^{-1}\left(\frac{3}{2}\phi_1^\star - 2\phi_1^n + \frac{1}{2}\phi_1^{n-1}\right), \psi\right)_Q + \left(\delta_{\phi_1} S\left(\phi_1^\star, \phi_2^\star\right), \psi\right)_Q \\
&+ \left(\delta_{\phi_1}\tilde{K}\left(\phi_1^\star, \phi_2^\star\right), \psi\right) + \left(\delta_{\phi_1} H\left(\check{\phi}_1^{n+1}, \check{\phi}_2^{n+1}\right), \psi\right)_Q + A\tau(\nabla(\phi_1^\star - \phi_1^n), \nabla\psi), \quad \forall\psi \in S_h.
\end{aligned} \tag{3.11}$$

Again, since $(\phi_1^\star + s\psi, \phi_2^\star) \in A_{h,\delta}$, the following direction is picked:

$$\psi = C_2\delta_{\alpha_1} - \delta_{\alpha_0},\ C_2 = \frac{\text{area}(D_{\alpha_0})}{\text{area}(D_{\alpha_1})}.$$

Similarly, an application of Lemma 3.1 results in an upper bound for the first term in (3.11), and the technical details are left to interested readers:

$$\frac{1}{D_1\tau}(-\Delta_h^{-1}(\frac{3}{2}\phi_1^\star - 2\phi_1^n + \frac{1}{2}\phi_1^{n-1}), \psi)_Q \leq \frac{4C_1}{3D_1\tau}\,\text{area}(D_{\alpha_0}). \tag{3.12}$$

The second term could also be similarly analyzed:

$$
\begin{aligned}
(\delta_{\phi_1} S(\phi_1^\star, \phi_2^\star), \psi)_Q =& \left(\frac{1}{\gamma} \ln(\frac{\alpha\phi_1^\star}{\gamma}) - \ln(1-\phi_1^\star-\phi_2^\star), \psi \right)_Q \\
=& \sum_{e\in\mathcal{T}_h} \left(\frac{1}{3} \triangle_e \sum_{j=1}^{3} \left(\frac{1}{\gamma} \ln(\frac{\alpha\phi_1^\star}{\gamma}) - \ln(1-\phi_1^\star-\phi_2^\star) \right) \psi(P_{e,j}) \right) \\
=& \frac{1}{3} \operatorname{area}(D_{\alpha_0}) \left(\left(\frac{1}{\gamma} \ln(\frac{\alpha\phi_1^\star}{\gamma}) - \ln(1-\phi_1^\star-\phi_2^\star) \right) |_{\alpha_1} \right. \\
& \left. - \left(\frac{1}{\gamma} \ln(\frac{\alpha\phi_1^\star}{\gamma}) - \ln(1-\phi_1^\star-\phi_2^\star) \right) |_{\alpha_0} \right) \\
=& \frac{1}{3} \operatorname{area}(D_{\alpha_0}) \Big(\ln \frac{(\phi_1^\star)^{\frac{1}{\gamma}}}{1-\phi_1^\star-\phi_2^\star} |_{\alpha_1} - \ln \frac{(\phi_1^\star)^{\frac{1}{\gamma}}}{1-\phi_1^\star-\phi_2^\star} |_{\alpha_0} \Big) \\
\leq& \frac{1}{3} \operatorname{area}(D_{\alpha_0}) \Big(\ln \frac{1}{1-\overline{\phi_1^0}-\overline{\phi_2^0}} - \ln \frac{(\frac{1}{3})^{1/\gamma}}{\delta} \Big).
\end{aligned}
\tag{3.13}
$$

Regarding the third term, a similar expansion enables one to derive the following bound, corresponding to (3.7):

$$
(\delta_{\phi_1} \tilde{K} (\phi_1^\star, \phi_2^\star), \psi) \leq \frac{(3a_1^2+a_3^2)C_{\mathcal{T}}}{24} \sum_{e\in D_{\alpha_0}} 1 + \frac{(a_1^2+3a_3^2)C_2 C_{\mathcal{T}}}{24} \sum_{e\in D_{\alpha_1}} 1. \tag{3.14}
$$

In terms of the concave term in (3.11), the following inequality could be similarly derived:

$$
(\delta_{\phi_1} H \left(\check{\phi}_1^{n+1}, \check{\phi}_2^{n+1} \right), \psi)_Q \leq \operatorname{area}(D_{\alpha_0})(\chi_{12} + 3\chi_{13} + \chi_{23}). \tag{3.15}
$$

For the artificial regularization term, the following estimate is valid:

$$
\begin{aligned}
& A\tau(\nabla(\phi_1^\star - \phi_1^n), \nabla\psi) \\
=& A\tau(\nabla(\phi_1^\star - \phi_1^n), \nabla\delta_{\alpha_0}) - A\tau C_2(\nabla(\phi_1^\star - \phi_1^n), \nabla\delta_{\alpha_1}) \\
\leq& A\tau \left(\sum_{e\in D_{\alpha_0}} \frac{h_e^2}{2\triangle_e} \sum_{i=1}^{3} \phi_1^\star(P_{e,i}) + C_2 \sum_{e\in D_{\alpha_1}} \frac{h_e^2}{2\triangle_e} \sum_{i=1}^{3} \phi_1^\star(P_{e,i}) \right) + 3C_{\mathcal{T}} A\tau \operatorname{area}(D_{\alpha_0}) \\
\leq& 6C_{\mathcal{T}} A\tau \operatorname{area}(D_{\alpha_0}).
\end{aligned}
$$

Subsequently, a summation of the above estimates leads to

$$
\begin{aligned}
& d_s \mathcal{J}^n (\phi_1^\star + s\psi, \phi_2^\star)|_{s=0} \leq \frac{1}{3} \operatorname{area}(D_{\alpha_0}) \ln\delta + r_1, \text{with} \\
r_1 =& \frac{1}{3} \operatorname{area}(D_{\alpha_0}) (\frac{4C_1}{D_1\tau} + \frac{1}{\gamma} \ln 3 + \ln \frac{1}{1-\overline{\phi_1^0}-\overline{\phi_2^0}} + 3\chi_{12} + 9\chi_{13} + 3\chi_{23} + 18C_{\mathcal{T}} A\tau) \\
& + \frac{(3a_1^2+a_3^2)C_{\mathcal{T}}}{24} \sum_{e\in D_{\alpha_0}} 1 + \frac{(a_1^2+3a_3^2)C_2 C_{\mathcal{T}}}{24} \sum_{e\in D_{\alpha_1}} 1.
\end{aligned}
$$

Again, r_1 is a constant for fixed τ and h, and δ could be chosen sufficiently small so that

$$
\frac{1}{3} \operatorname{area}(D_{\alpha_0}) \ln\delta + r_1 < 0. \tag{3.16}
$$

A typical choice could be $\delta = \min\{\exp\left(-\frac{3(r_1+1)}{\text{area}(D_{\alpha_0})}\right), \frac{1}{3}\}$. Therefore, we obtain the following inequality

$$d_{\text{s}}\mathcal{J}^n\left(\phi_1^\star + s\psi, \phi_2^\star\right)|_{s=0} < 0.$$

This contradicts the assumption that $\mathcal{J}^n$ has a minimum at $(\phi_1^\star, \phi_2^\star)$, since the directional derivative is negative in a direction pointing into $(A_{h,\delta})^\circ$, the interior of $A_{h,\delta}$.

Case 4: The global minimum of $\mathcal{J}^n$ over $\mathcal{A}_{h,\delta}$ could not occur on the functional boundary point where $\phi_{1,\alpha_0}^\star + \phi_{2,\alpha_0}^\star = \delta$, if δ is sufficiently small, for any point index α_0. This analysis is based on similar arguments as in the previous case, and the details are left to the interested readers.

Finally, a combination of these four cases reveals that, the global minimizer of $\mathcal{J}^n(\phi_1, \phi_2)$ could only possibly occur at interior point of $(A_{h,\delta})^\circ \subset A_h^\circ$. Because of the smoothness of $\mathcal{J}^n$ in terms of ϕ_1 and ϕ_2, there must be a solution $(\phi_1, \phi_2) \in A_h^\circ$ that minimizes $\mathcal{J}^n(\phi_1, \phi_2)$ over A_h. Such a minimization function is exactly equivalent to the numerical solution of (2.4). In turn, the existence of the numerical solution has been proved.

Moreover, since $\mathcal{J}^n(\phi_1, \phi_2)$ is a strictly convex function over A_h, the uniqueness analysis for this numerical solution is straightforward. This finishes the proof of Theorem 3.1. □

3.2 Energy stability

Energy stability of a high-order numerical scheme turns out to be a challenging issue. Such an energy stability for the proposed numerical scheme (2.4) is stated below.

Theorem 3.2. *The unique solution of the proposed fully-discrete scheme* (2.4) *is energy stable. In more details, for any time step size* $\tau > 0$, *when* $A \geq \max\{\frac{D_1(\chi_{12}+3\chi_{13}+\chi_{23})^2}{16}, \frac{D_2(\chi_{12}+\chi_{13}+3\chi_{23})^2}{16}\}$, *the following estimate is available:*

$$\tilde{E}(\phi_{1h}^{n+1}, \phi_{2h}^{n+1}) \leq \tilde{E}(\phi_{1h}^n, \phi_{2h}^n)$$

with

$$\begin{aligned}\tilde{E}(\phi_{1h}^{n+1}, \phi_{2h}^{n+1}) =& \hat{E}(\phi_{1h}^{n+1}, \phi_{2h}^{n+1}) + \frac{1}{4\tau D_1}\left\|\phi_{1h}^{n+1} - \phi_{1h}^n\right\|_{-1,Q}^2 + \frac{1}{4\tau D_2}\left\|\phi_{2h}^{n+1} - \phi_{2h}^n\right\|_{-1,Q}^2 \\ &+ \frac{\chi_{12}+3\chi_{13}+\chi_{23}}{2}\|\phi_{1h}^{n+1} - \phi_{1h}^n\|_Q^2 + \frac{\chi_{12}+\chi_{13}+3\chi_{23}}{2}\|\phi_{2h}^{n+1} - \phi_{2h}^n\|_Q^2.\end{aligned}$$

Proof. For $w_1, w_2 \in \mathring{S}_h$, we denote $v_1 = (-\Delta_h)^{-1}w_1, v_2 = (-\Delta_h)^{-1}w_2$. In turn, the following equations could be obtained:

$$\begin{aligned}&\left(\frac{\frac{3}{2}\phi_{1h}^{n+1} - 2\phi_{1h}^n + \frac{1}{2}\phi_{1h}^{n-1}}{D_1\tau}, (-\Delta_h)^{-1}w_1\right) + \left(\delta_{\phi_1}\tilde{K}(\phi_{1h}^{n+1}, \phi_{2h}^{n+1}), w_1\right) \\ &+ \left(\frac{\partial}{\partial\phi_1}S(\phi_{1h}^{n+1}, \phi_{2h}^{n+1}) + \frac{\partial}{\partial\phi_1}H(\check{\phi}_{1h}^{n+1}, \check{\phi}_{2h}^{n+1}), w_1\right)_Q + A\tau(\nabla(\phi_{1h}^{n+1} - \phi_{1h}^n), \nabla w_1) = 0, \\ &\left(\frac{\frac{3}{2}\phi_{2h}^{n+1} - 2\phi_{2h}^n + \frac{1}{2}\phi_{2h}^{n-1}}{D_2\tau}, (-\Delta_h)^{-1}w_2\right) + \left(\delta_{\phi_2}\tilde{K}(\phi_{1h}^{n+1}, \phi_{2h}^{n+1}), w_2\right) \\ &+ \left(\frac{\partial}{\partial\phi_2}S(\phi_{1h}^{n+1}, \phi_{2h}^{n+1}) + \frac{\partial}{\partial\phi_2}H(\check{\phi}_{1h}^{n+1}, \check{\phi}_{2h}^{n+1}), w_2\right)_Q + A\tau(\nabla(\phi_{2h}^{n+1} - \phi_{2h}^n), \nabla w_2) = 0.\end{aligned} \tag{3.17}$$

Meanwhile, we set $w_1 = \phi_{1h}^{n+1} - \phi_{1h}^n, w_2 = \phi_{2h}^{n+1} - \phi_{2h}^n$ in (3.17). An application of Lemma 2.2 indicates that

$$
\begin{aligned}
0 =& \frac{3}{2D_1\tau}\|\phi_{1h}^{n+1} - \phi_{1h}^n\|_{-1,Q}^2 - \frac{1}{2D_1\tau}(\phi_{1h}^{n+1} - \phi_{1h}^n, \phi_{1h}^n - \phi_{1h}^{n-1})_{-1,Q} \\
&+ \left(\frac{\partial}{\partial\phi_1}S(\phi_{1h}^{n+1}, \phi_{2h}^{n+1}) + \frac{\partial}{\partial\phi_1}H(\check{\phi}_{1h}^{n+1}, \check{\phi}_{2h}^{n+1}), \phi_{1h}^{n+1} - \phi_{1h}^n\right)_Q + A\tau\|\nabla(\phi_{1h}^{n+1} - \phi_{1h}^n)\|^2 \\
&+ \frac{3}{2D_2\tau}\|\phi_{2h}^{n+1} - \phi_{2h}^n\|_{-1,Q}^2 - \frac{1}{2D_2\tau}(\phi_{2h}^{n+1} - \phi_{2h}^n, \phi_{2h}^n - \phi_{2h}^{n-1})_{-1,Q} \\
&+ \left(\frac{\partial}{\partial\phi_2}S(\phi_{1h}^{n+1}, \phi_{2h}^{n+1}) + \frac{\partial}{\partial\phi_2}H(\check{\phi}_{1h}^{n+1}, \check{\phi}_{2h}^{n+1}), \phi_{2h}^{n+1} - \phi_{2h}^n\right)_Q + A\tau\|\nabla(\phi_{2h}^{n+1} - \phi_{2h}^n)\|^2 \\
&+ \left(\delta_{\phi_1}\tilde{K}(\phi_{1h}^{n+1}, \phi_{2h}^{n+1}), \phi_{1h}^{n+1} - \phi_{1h}^n\right) + \left(\delta_{\phi_2}\tilde{K}(\phi_{1h}^{n+1}, \phi_{2h}^{n+1}), \phi_{2h}^{n+1} - \phi_{2h}^n\right) \\
\geq& \frac{5}{4D_1\tau}\|\phi_{1h}^{n+1} - \phi_{1h}^n\|_{-1,Q}^2 - \frac{1}{4D_1\tau}\|\phi_{1h}^n - \phi_{1h}^{n-1}\|_{-1,Q}^2 + A\tau\|\nabla(\phi_{1h}^{n+1} - \phi_{1h}^n)\|^2 \\
&+ \frac{5}{4D_2\tau}\|\phi_{2h}^{n+1} - \phi_{2h}^n\|_{-1,Q}^2 - \frac{1}{4D_2\tau}\|\phi_{2h}^n - \phi_{2h}^{n-1}\|_{-1,Q}^2 + A\tau\|\nabla(\phi_{2h}^{n+1} - \phi_{2h}^n)\|^2 \\
&+ \left(\frac{\partial}{\partial\phi_1}H(\check{\phi}_{1h}^{n+1}, \check{\phi}_{2h}^{n+1}), \phi_{1h}^{n+1} - \phi_{1h}^n\right)_Q + \left(\frac{\partial}{\partial\phi_2}H(\check{\phi}_{1h}^{n+1}, \check{\phi}_{2h}^{n+1}), \phi_{2h}^{n+1} - \phi_{2h}^n\right)_Q \\
&- \left(\frac{\partial}{\partial\phi_1}H(\phi_{1h}^n, \phi_{2h}^n), \phi_{1h}^{n+1} - \phi_{1h}^n\right)_Q - \left(\frac{\partial}{\partial\phi_2}H(\phi_{1h}^n, \phi_{2h}^n), \phi_{2h}^{n+1} - \phi_{2h}^n\right)_Q \\
&+ \hat{E}(\phi_{1h}^{n+1}, \phi_{2h}^{n+1}) - \hat{E}(\phi_{1h}^n, \phi_{2h}^n).
\end{aligned}
$$

On the other hand, an application of the Cauchy inequality gives the following bound:

$$
\frac{1}{D_i\tau}\|\phi_{ih}^{n+1} - \phi_{ih}^n\|_{-1,h}^2 + A\tau\|\nabla(\phi_{ih}^{n+1} - \phi_{ih}^n)\|^2 \geq 2\frac{A^{1/2}}{D_i^{1/2}}\|\phi_{ih}^{n+1} - \phi_{ih}^n\|_Q^2, \quad i = 1, 2
$$

and we have

$$
\begin{aligned}
&\left(\frac{\partial}{\partial\phi_1}H(\check{\phi}_{1h}^{n+1}, \check{\phi}_{2h}^{n+1}), \phi_{1h}^{n+1} - \phi_{1h}^n\right)_Q + \left(\frac{\partial}{\partial\phi_2}H(\check{\phi}_{1h}^{n+1}, \check{\phi}_{2h}^{n+1}), \phi_{2h}^{n+1} - \phi_{2h}^n\right)_Q \\
&- \left(\frac{\partial}{\partial\phi_1}H(\phi_{1h}^n, \phi_{2h}^n), \phi_{1h}^{n+1} - \phi_{1h}^n\right)_Q - \left(\frac{\partial}{\partial\phi_2}H(\phi_{1h}^n, \phi_{2h}^n), \phi_{2h}^{n+1} - \phi_{2h}^n\right)_Q \\
=& \left(-2\chi_{13}(\phi_{1h}^n - \phi_{1h}^{n-1}) + (\chi_{12} - \chi_{13} - \chi_{23})(\phi_{2h}^n - \phi_{2h}^{n-1}), \phi_{1h}^{n+1} - \phi_{1h}^n\right)_Q \\
&+ \left(-2\chi_{23}(\phi_{2h}^n - \phi_{2h}^{n-1}) + (\chi_{12} - \chi_{13} - \chi_{23})(\phi_{1h}^n - \phi_{1h}^{n-1}), \phi_{2h}^{n+1} - \phi_{2h}^n\right)_Q \\
=& -2\chi_{13}\cdot\frac{1}{2}\left(\|\phi_{1h}^n - \phi_{1h}^{n-1}\|_Q^2 - \|\phi_{1h}^{n+1} - 2\phi_{1h}^n + \phi_{1h}^{n-1}\|_Q^2 + \|\phi_{1h}^{n+1} - \phi_{1h}^n\|_Q^2\right) \\
&+ \frac{1}{2}(\chi_{12} - \chi_{13} - \chi_{23})\left(\|\phi_{2h}^n - \phi_{2h}^{n-1}\|_Q^2 - \|\phi_{1h}^{n+1} - \phi_{1h}^n - \phi_{2h}^n + \phi_{2h}^{n-1}\|_Q^2 + \|\phi_{1h}^{n+1} - \phi_{1h}^n\|_Q^2\right) \\
&- 2\chi_{23}\cdot\frac{1}{2}\left(\|\phi_{2h}^n - \phi_{2h}^{n-1}\|_Q^2 - \|\phi_{2h}^{n+1} - 2\phi_{2h}^n + \phi_{2h}^{n-1}\|_Q^2 + \|\phi_{2h}^{n+1} - \phi_{2h}^n\|_Q^2\right) \\
&+ \frac{1}{2}(\chi_{12} - \chi_{13} - \chi_{23})\left(\|\phi_{1h}^n - \phi_{1h}^{n-1}\|_Q^2 - \|\phi_{2h}^{n+1} - \phi_{2h}^n - \phi_{1h}^n + \phi_{1h}^{n-1}\|_Q^2 + \|\phi_{2h}^{n+1} - \phi_{2h}^n\|_Q^2\right) \\
=& -2\chi_{13}\cdot\frac{1}{2}\left(\|\phi_{1h}^n - \phi_{1h}^{n-1}\|_Q^2 + \|\phi_{1h}^{n+1} - \phi_{1h}^n\|_Q^2\right) - \frac{\chi_{13} + \chi_{23}}{2}\left(\|\phi_{2h}^n - \phi_{2h}^{n-1}\|_Q^2 + \|\phi_{1h}^{n+1} - \phi_{1h}^n\|_Q^2\right) \\
&- \frac{\chi_{12}}{2}\|\phi_{1h}^{n+1} - \phi_{1h}^n - \phi_{2h}^n + \phi_{2h}^{n-1}\|_Q^2 - 2\chi_{23}\cdot\frac{1}{2}\left(\|\phi_{2h}^n - \phi_{2h}^{n-1}\|_Q^2 + \|\phi_{2h}^{n+1} - \phi_{2h}^n\|_Q^2\right)
\end{aligned}
$$

$$
\begin{aligned}
&-\frac{\chi_{13}+\chi_{23}}{2}\left(\|\phi_{1h}^{n}-\phi_{1h}^{n-1}\|_{Q}^{2}+\|\phi_{2h}^{n+1}-\phi_{2h}^{n}\|_{Q}^{2}\right)-\frac{\chi_{12}}{2}\|\phi_{2h}^{n+1}-\phi_{2h}^{n}-\phi_{1h}^{n}+\phi_{1h}^{n-1}\|_{Q}^{2}\\
\geq&-\frac{\chi_{12}+3\chi_{13}+\chi_{23}}{2}\|\phi_{1h}^{n}-\phi_{1h}^{n-1}\|_{Q}^{2}-\frac{\chi_{12}+\chi_{13}+3\chi_{23}}{2}+\|\phi_{2h}^{n+1}-\phi_{2h}^{n}\|_{Q}^{2}\\
&-\frac{\chi_{12}+3\chi_{13}+\chi_{23}}{2}\|\phi_{1h}^{n+1}-\phi_{1h}^{n}\|_{Q}^{2}-\frac{\chi_{12}+\chi_{13}+3\chi_{23}}{2}+\|\phi_{2h}^{n+1}-\phi_{2h}^{n}\|_{Q}^{2}.
\end{aligned}
$$

A summation leads to

$$
\begin{aligned}
&\hat{E}(\phi_{1h}^{n+1},\phi_{2h}^{n+1})-\hat{E}(\phi_{1h}^{n},\phi_{2h}^{n})+\frac{1}{4D_1\tau}(\|\phi_{1h}^{n+1}-\phi_{1h}^{n}\|_{-1,Q}^{2}-\|\phi_{1h}^{n}-\phi_{1h}^{n-1}\|_{-1,Q}^{2})\\
&+\frac{1}{4D_2\tau}(\|\phi_{2h}^{n+1}-\phi_{2h}^{n}\|_{-1,Q}^{2}-\|\phi_{2h}^{n}-\phi_{2h}^{n-1}\|_{-1,Q}^{2})\\
&-\frac{\chi_{12}+3\chi_{13}+\chi_{23}}{2}(\|\phi_{1h}^{n}-\phi_{1h}^{n-1}\|_{Q}^{2}-\|\phi_{1h}^{n+1}-\phi_{1h}^{n}\|_{Q}^{2})\\
&-\frac{\chi_{12}+\chi_{13}+3\chi_{23}}{2}(\|\phi_{2h}^{n}-\phi_{2h}^{n-1}\|_{Q}^{2}-\|\phi_{2h}^{n+1}-\phi_{2h}^{n}\|_{Q}^{2})\\
\leq&(-2\frac{A^{1/2}}{D_1^{1/2}}+\frac{\chi_{12}+3\chi_{13}+\chi_{23}}{2})\|\phi_{1h}^{n+1}-\phi_{1h}^{n}\|_{Q}^{2}+(-2\frac{A^{1/2}}{D_2^{1/2}}+\frac{\chi_{12}+\chi_{13}+3\chi_{23}}{2})\|\phi_{2h}^{n+1}-\phi_{2h}^{n}\|_{Q}^{2}.
\end{aligned}
$$

Finally, let $A \geq \max\{\frac{D_1(\chi_{12}+3\chi_{13}+\chi_{23})^2}{16}, \frac{D_2(\chi_{12}+\chi_{13}+3\chi_{23})^2}{16}\}$, we get the desired result. □

Remark 3.2. *Because of the three-level nature in the numerical structure, the proposed numerical scheme* (2.4) *only preserves the dissipation property of a modified energy, composed of the original energy functional and a few numerical correction terms, and these correction terms of order $O(\tau)$ and $O(\tau^2)$. In fact, for a few singular potential gradient flow models without a concave part in the free energy expansion, such as the Poisson-Nernst-Planck (PNP) system, the original energy dissipative numerical schemes have been carefully studied in recent years. For example, a modified second-order Crank-Nicolson nonlinear approximation to the logarithmic term, in the form of $\frac{F(\phi^{n+1})-F(\phi^n)}{\phi^{n+1}-\phi^n}$, is proposed in [32], and the original energy dissipation is proved. Meanwhile, the denominator of the quotient term becomes problematic when the system approaches the steady state. To remedy this issue, Ding et al [12] proposed a finite volume algorithm based on a modified second-order Crank-Nicolson technique for modified PNP equations. A similar work is reported in [11] for the Patlak-Keller-Segel system.*

On the other hand, it is noticed that, all these original energy dissipative numerical schemes correspond to a free energy without any concave part. In turn, the strictly convex nature of the full free energy enables a second order accurate, two-level approximation to the chemical potential, so that the original free energy dissipation could be theoretically derived. In comparison, the ternary MMC free energy expansion (1.1) *contains a concave part, namely the mixing entropy $H(\phi_1, \phi_2)$. In turn, a two-level, second order accurate and original free energy dissipative approximation to the chemical potential is not available by a direct calculation, and the energy stability estimate has to be in terms of a numerically corrected energy functional, which comes from the three-level nature of the proposed numerical scheme. A second order accurate, original energy dissipative numerical scheme to the ternary MMC system will be explore in our future works.*

4 Numerical results

In this section, we present three numerical examples to illustrate some theoretical properties, such as mass conservation, energy dissipation and positivity-preserving. In addition, we test the convergence rate and the influence of the initial concentration. All parameters are fixed shown in Table 1, except the special statement.

Table 1: The values of the parameters in the simulation

Parameter	D_1	D_2	χ_{12}	χ_{13}	χ_{23}	γ	N	a_1	a_2	a_3
Value	1	1	4	10	1.6	0.16	5.12	1	1	1

Example 4.1. *(Convergence test) Consider the domain* $\Omega = (0,1)^2$. *Set statistical segment length of the* i*-th component* $a_i = 0.3,\ i = 1,2,3$. *The initial conditions are given by*

$$\begin{aligned} \phi_1(x,y,0) &= 0.1 + 0.01\cos(2\pi x)\cos(2\pi y), \\ \phi_2(x,y,0) &= 0.5 + 0.01\cos(2\pi x)\cos(2\pi y). \end{aligned} \tag{4.1}$$

In order to test the second order convergence, we use a linear ratio of h and τ, *i.e.*, $\tau = Ch, C = 0.002$. At the final time $T = 0.02$, we expect the global error to be of order $\mathcal{O}(\tau^2) + \mathcal{O}(h^2) = \mathcal{O}(h^2)$ in the ℓ^2 and ℓ^∞ norms, as $h, \tau \to 0$. Due to the fact an explicit form of the exact solution is not available, instead of calculating the error at the final time, we compute the Cauchy difference, which is defined as $\delta_\phi := \phi_{h_f} - \mathcal{I}_c^f(\phi_{h_c})$, and $\mathcal{I}_c^f$ is a bilinear interpolation operator (with an application of Nearest Neighbor Interpolation in Matlab, see [3]). Moreover, ϕ_{h_c} is a coarse solution and ϕ_{h_f} is a fine solution, where $h_c = 2h_f$ are needed at the same final time. The ℓ^2 and ℓ^∞ norms of Cauchy difference and the convergence rates with different stability factors, $A = 0, 64, 100$, are displayed in Figure 1. The results confirm the expectation for the convergence order. In addition, it is discovered that the convergence rate is independent of the stability factor values. In particular, the numerical error is the smallest when $A = 0$, which is consistent with the fact that the extra regularization term vanishes.

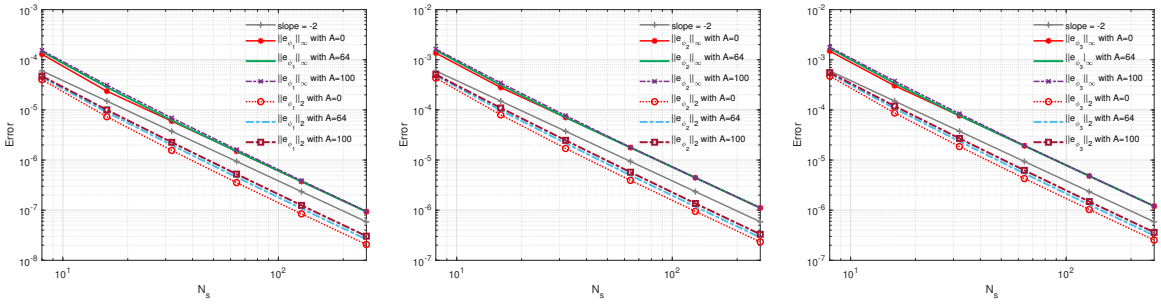

Figure 1: The ℓ^2 and ℓ^∞ errors versus spatial resolution N_s with different stabilizer factor values, $A = 0, 64, 100$. The parameters are given by $T = 0.02$, $a_i = 0.3$ and $\tau = 0.002h$. The reference line has an exact slope of -2.

Example 4.2. *(Influence of the stability factor value) The initial data is set as*

$$\begin{aligned} \phi_1(x, y, 0) &= 0.1 + r_{i,j} \\ \phi_2(x, y, 0) &= 0.5 + r_{i,j} \end{aligned} \tag{4.2}$$

where $r_{i,j}$ are uniformly distributed random numbers in $[-0.01, 0.01]$.

This example is designed to investigate the influence of stability factor value on energy stability. In Figure 2, a dissipation of the free energy is observed for all values of stability factor: $A = 0, 1, 10, 64, 100$. Meanwhile, a careful examination of the energy evolutionary curve reveals that there is a slight increase of the free energy at the beginning of the time evolution, for $A = 0, 1$ and 10. Therefore, we will select stability factor $A = 64$ in the following example. With a larger time evolution scale, the energy evolution is displayed in Figure 3, which indicates that the free energy keeps dissipative. In Figures 4 and 5, we present the evolution curves of the total mass error, the maximum values and minimum values of ϕ_1, ϕ_2 and ϕ_3, respectively. It is obvious that the numerical solution satisfies mass conservation and positivity preserving properties, which is consistent with the theory analysis, i.e., $0 < \phi_i < 1$. Moreover, the numerical solutions of ϕ_1, ϕ_2 and ϕ_3 at a sequence of time instants are displayed in Figure 6, which match the existing binary MMC results.

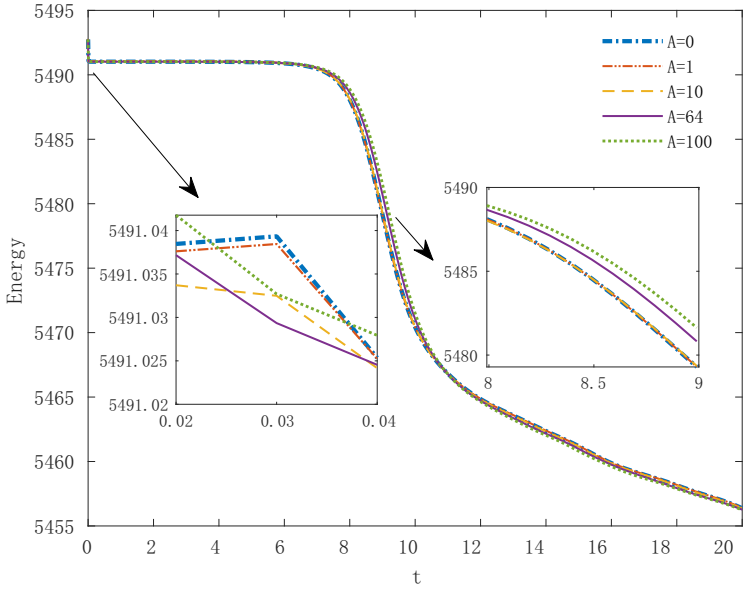

Figure 2: Evolution plots of the energy over time with different stability factor values of A, with the initial data given by (4.2).

Example 4.3. *(Influence of the initial concentration) Let $\Omega = (0, 50)^2$, and a random initial perturbation is included in the initial data:*

$$\begin{aligned} \phi_1(x, y, 0) &= \phi_{10} + r_{i,j}, \\ \phi_2(x, y, 0) &= \phi_{20} + r_{i,j}. \end{aligned} \tag{4.3}$$

where the $r_{i,j}$ are uniformly distributed random numbers in $[-0.01, 0.01]$.

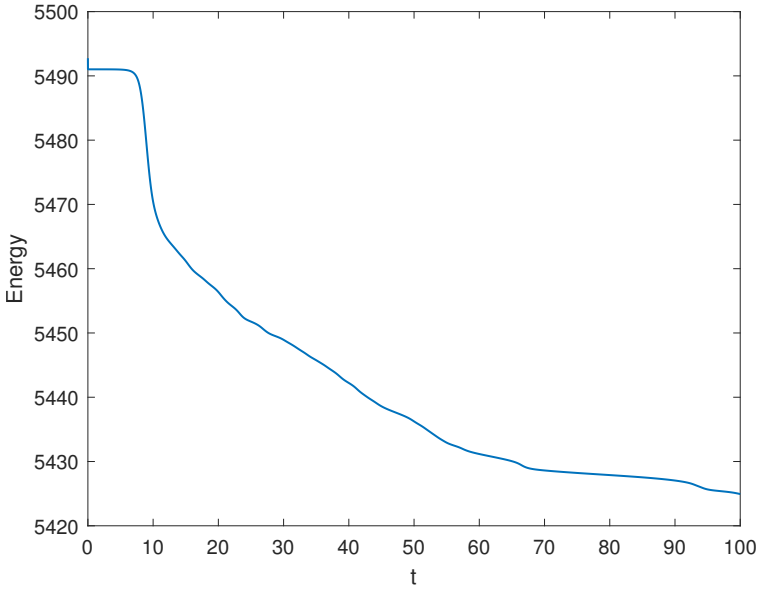

Figure 3: Evolution of the energy over time, with the initial data given by (4.2).

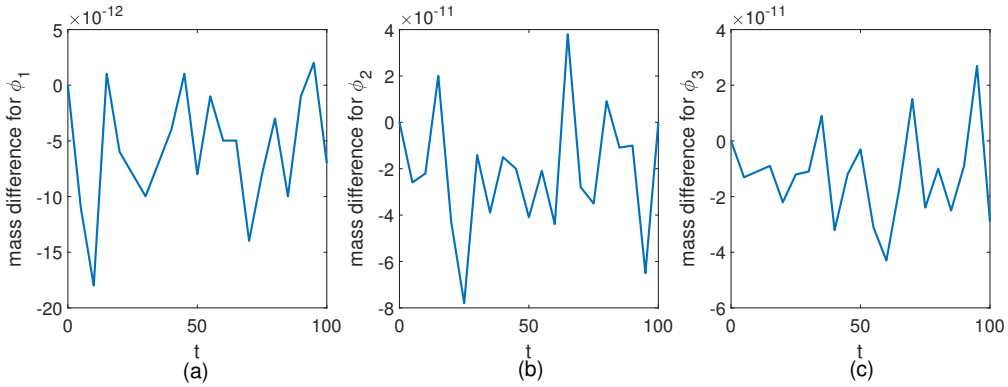

Figure 4: The error development of the total mass for ϕ_1, ϕ_2 and ϕ_3, with the initial data given by (4.2).

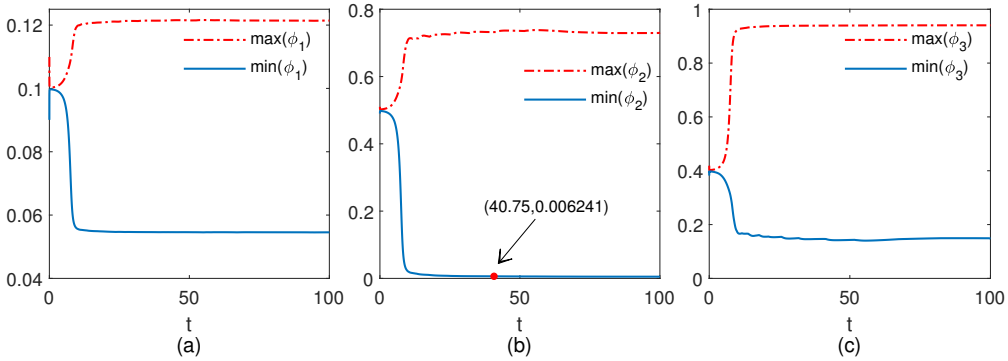

Figure 5: The time evolution of the maximum and minimum values for ϕ_1, ϕ_2 and ϕ_3, with the initial data given by (4.2).

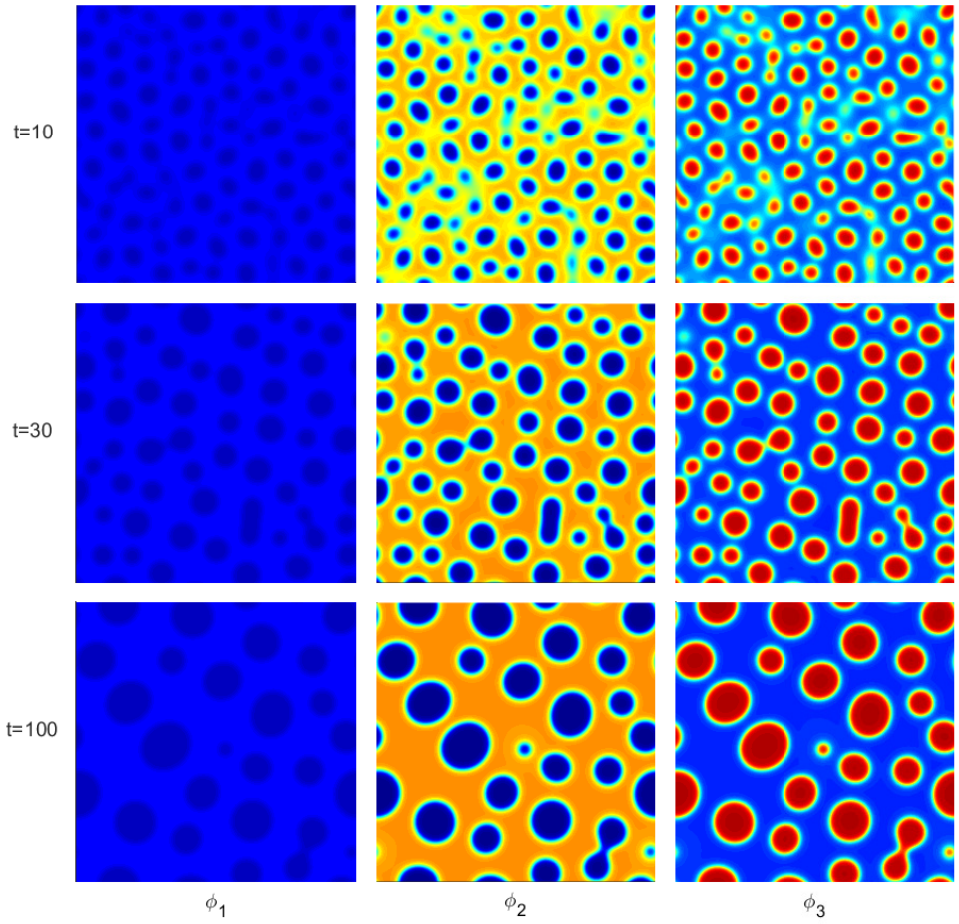

Figure 6: Evolution of three phase variables at $t = 10, 30, 100$, with the initial data given by (4.3).

This example aims to study the influence of the different initial profiles on the phase transition of MMC hydrogels. In Figure 7, the four columns of the graph are taken with $\phi_{20} = 0.2, 0.3, 0.4, 0.5$, when $\phi_{10} = 0.1$ is fixed. The three rows of the graph are associated with the volume fraction variable ϕ_1, ϕ_2 and ϕ_3, respectively. The light blue domain in the first row, corresponding to the larger values of ϕ_1, represents the higher concentration of MMCs. The yellow domain in the second row, corresponding to the larger values of ϕ_2, stands for the concentrated polymer segments. The red domain in the third row, corresponding to the larger values of ϕ_3, is connected with the higher concentration. From the second row, some facts could be clearly observed: there is only isolated yellow ball or chain at $\phi_{20} = 0.2$ and 0.3, which indicates that the mixture fails to form a network due to insufficient concentration of the polymer chains; a large area of yellow appears at $\phi_{20} = 0.4$ and 0.5, and this fact means that initial concentration of the polymer chain is sufficient to form a reticular structure. This simulation result is consistent with the ones reported in [27]. If $\phi_{20} = 0.5$ is fixed, the snapshot plots at $T = 40$, with four different values of ϕ_{10}, are presented in Figure 8. This implies that when the polymer chain concentration is sufficiently high, the formation of the mixture network structure is independent of the concentration of MMCs.

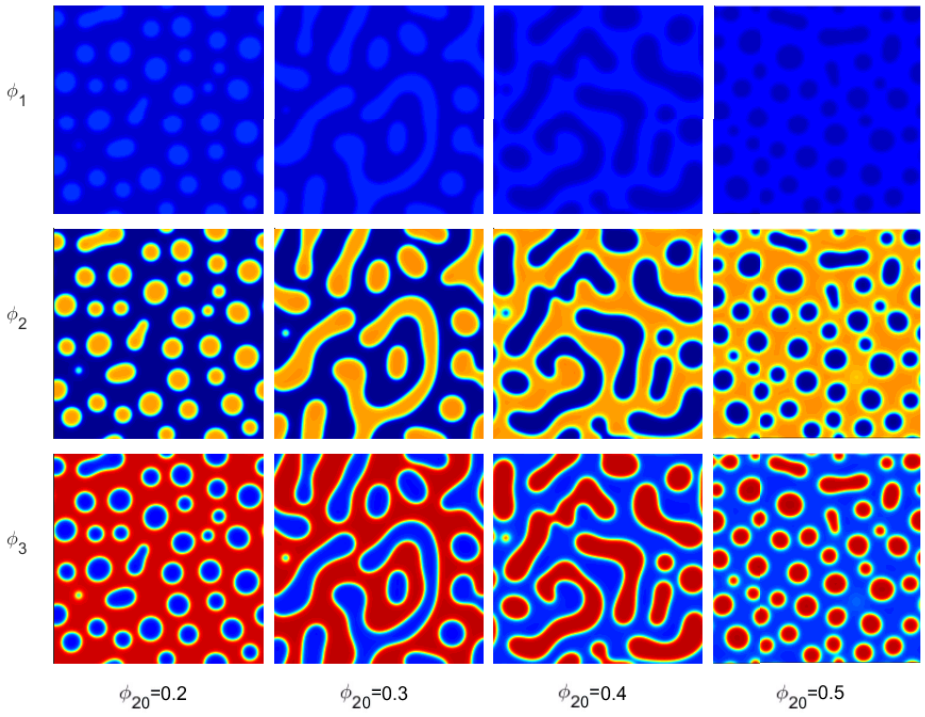

Figure 7: The phase plots of three variables with different values of ϕ_{20} at $T = 40$, and the initial data is given by (4.3).

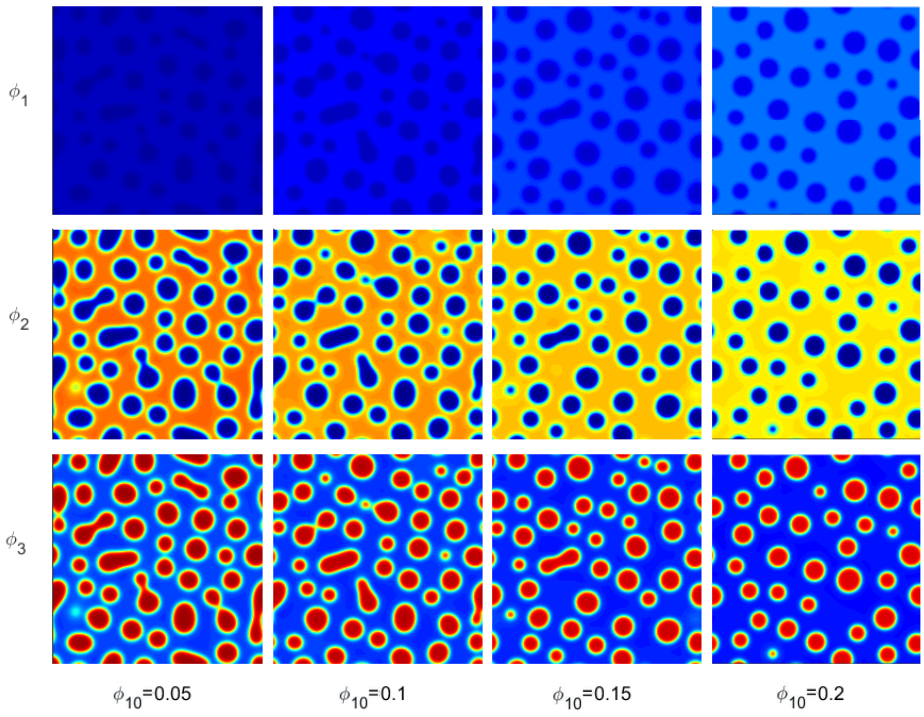

Figure 8: The phase plots of three variables with different values of ϕ_{10} at $T = 40$, and the initial data is given by (4.3).

5 Conclusions

In this paper, we have developed a second order accurate, BDF-style numerical scheme for the three-component Cahn-Hilliard flow model in macromolecular microphere composite hydrogels, with a mass lumped finite element spatial approximation. Based on the singular nature of the Flory-Huggins free energy and the surface diffusion coefficients as the phase variables approach to the limiting values, the unique solvability and positivity preserving analysis has been theoretically justified. In addition, a modified energy stability analysis has also been derived, with the help of the convex-concave decomposition of the free energy, combined with convexity analysis. Furthermore, a few numerical examples are presented, which verifies the mass conservation, free energy dissipation, as well as the second order convergence rate. We have also investigated the influence of different stability factor values and different initial data on the phase transition process in the numerical simulations.

Acknowledgments

M.Q. Yuan is partially supported by the Research Foundation of China University of Petroleum-Beijing at Karamay (No. XQZX20230030) and Talent Project of Tianchi Doctoral Program in Xinjiang Uygur Autonomous Region. L.X. Dong is partially supported by the National Natural Science Foundation of China (No. 12201051). C. Wang is partially supported by the National Science Foundation (No. DMS-2012269, DMS-2309548).

References

[1] W. Chen, Y. Liu, C. Wang, and S. Wise. An optimal-rate convergence analysis of a fully discrete finite difference scheme for Cahn-Hilliard-Hele-Shaw equation. *Math. Comput.*, 85:2231–2257, 2016.

[2] W. Chen, C. Wang, S. Wang, X. Wang, and S. Wise. Energy stable numerical schemes for a ternary Cahn-Hilliard system. *J. Sci. Comput.*, 84:27, 2020.

[3] W. Chen, C. Wang, X. Wang, and S. Wise. Positivity-preserving, energy stable numerical schemes for the Cahn-Hilliard equation with logarithmic potential. *J. Comput. Phys. X*, 3:100031, 2019.

[4] X. Chen, C. Wang, and S. Wise. A preconditioned steepest descent solver for the Cahn-Hilliard equation with variable mobility. *Int. J. Numer. Anal. Model.*, 19(8):839–863, 2022.

[5] K. Cheng, C. Wang, S. Wise, and Y. Wu. A third order accurate in time BDF-type energy stable scheme for the Cahn-Hilliard equation. *Numer. Math. Theor. Meth. Appl.*, 15:279–303, 2022.

[6] Q. Cheng, C. Liu, and J. Shen. A new lagrange multiplier approach for gradient flows. *Comput. Method Appl. M.*, 367:113070, 2020.

[7] Q. Cheng and J. Shen. A new lagrange multiplier approach for constructing structure preserving schemes, ii. bound preserving. *SIAM J. Numer. Anal.*, 60(3):970–998, 2022.

[8] A. Christlieb, J. Jones, J. Promislow, K. Wetton, B. Willoughby, and Mark. High accuracy solutions to energy gradient flows from material science models. *J. Comput. Phys.*, 257:193–215, 2014.

[9] Z. Qiao D. Hou and T. Tang. Fast high order and energy dissipative schemes with variable time steps for time-fractional Molecular Beam Epitaxial Growth model. *Ann. Appl. Math.*, 39:429–461, 2023.

[10] P. deGennes. Dynamics of fluctuations and spinodal decomposition in polymer blends. *J. Chem. Phys.*, 72:4756–4763, 1980.

[11] J. Ding, C. Wang, and S. Zhou. A second-order accurate, original energy dissipative numerical scheme for chemotaxis and its convergence analysis. *Math. Comp.*, 2025. accepted and in press.

[12] J. Ding and S. Zhou. Second-order, and unconditional energy dissipative scheme for modified Poisson-Nernst-Planck equations. *J. Comput. Phys.*, 510:113094, 2024.

[13] L. Dong, W. Feng, C. Wang, S. Wise, and Z. Zhang. Convergence analysis and numerical implementation of a second order numerical scheme for the three-dimensional phase field crystal equation. *Comput. Math. Appl.*, 75:1912–1928, 2018.

[14] L. Dong, C. Wang, S. Wise, and Z. Zhang. A positivity-preserving, energy stable scheme for a ternary Cahn-Hilliard system with the singular interfacial parameters. *J. Comput. Phys.*, 442:110451, 2021.

[15] L. Dong, C. Wang, S. Wise, and Z. Zhang. Optimal rate convergence analysis of a numerical scheme for the ternary Cahn-Hilliard system with a Flory-Huggins-deGennes energy potential. *J. Comput. Appl. Math.*, 415:114474, 2022.

[16] L. Dong, C. Wang, H. Zhang, and Z. Zhang. A positivity-preserving, energy stable and convergent numerical scheme for the Cahn-Hilliard equation with a Flory-Huggins-deGennes energy. *Commun. Math. Sci.*, 17(4):921–939, 2019.

[17] L. Dong, C. Wang, H. Zhang, and Z. Zhang. A positivity-preserving second-order BDF scheme for the Cahn-Hilliard equation with variable interfacial parameters. *Commun. Comput. Phys.*, 28(3):967–998, 2020.

[18] L. Dong, C. Wang, and Z. Zhang. A positivity-preserving, second-order energy stable and convergent numerical scheme for a ternary system of macromolecular microsphere composite hydrogels. *J. Comput. Appl. Math*, 462:116463, 2025.

[19] J. Drury and D. Mooney. Hydrogels for tissue engineering: scaffold design variables and applications. *Biomaterials*, 24(24):4337–4351, 2003.

[20] D. Eyre. Unconditionally gradient stable time marching the Cahn-Hilliard equation. In J. W. Bullard, R. Kalia, M. Stoneham, and L.Q. Chen, editors, *Computational and Mathematical Models of Microstructural Evolution*, volume 53, pages 1686–1712, Warrendale, PA, USA, 1998. Materials Research Society.

[21] W. Feng, A. Salgado, C. Wang, and S. Wise. Preconditioned steepest descent methods for some nonlinear elliptic equations involving p-Laplacian terms. *J. Comput. Phys.*, 334:45–67, 2017.

[22] W. Feng, C. Wang, S. Wise, and Z. Zhang. A second-order energy stable backward differentiation formula method for the epitaxial thin film equation with slope selection. *Numer. Meth. Part. D. E.*, 34:1975–2007, 2018.

[23] Q. Hong, Y. Gong, and J. Zhao. A physics-informed structure-preserving numerical scheme for the phase-field hydrodynamic model of ternary fluid flows. *Numer. Math. Theor. Meth. Appl.*, 16:565–596, 2023.

[24] B. Hou, M. Yuan, and P. Huang. Fully discrete scheme for a time-dependent Ginzburg-Landau equation in macromolecular microspheres composite hydrogels. *Comput. Math. Appl.*, 151:127–133, 2023.

[25] D. Hou and Z. Qiao. A linear adaptive second-order backward differentiation formulation scheme for the phase field crystal equation. *Numer. Meth. Part. D. E.*, 39:4174–4195, 2023.

[26] T. Huang, H. Xu, K. Jiao, L. Zhu, H. Brown, and H. Wang. A novel hydrogel with high mechanical strength: A macromolecular microsphere composite hydrogel. *Adv. Mater.*, 19(12):1622–1626, 2007.

[27] G. Ji, Y. Yang, and H. Zhang. Modeling and simulation of a ternary system for macromolecular microsphere composite hydrogels. *East Asian J. Appl. Math.*, 11(1):93–118, 2021.

[28] D. Li and Z. Qiao. On second order semi-implicit fourier spectral methods for 2D Cahn-Hilliard equations. *J. Sci. Comput.*, 70:301–341, 2017.

[29] X. Li, G. Ji, and H. Zhang. Phase transitions of macromolecular microsphere composite hydrogels based on the stochastic Cahn-Hilliard equation. *J. Comput. Phys.*, 283:81–97, 2015.

[30] X. Li, Z. Qiao, and H. Zhang. An unconditionally energy stable finite difference scheme for a stochastic Cahn-Hilliard equation. *Sci. China Math.*, 59(9):1815–1834, 2016.

[31] C. Liu, C. Wang, S. Wise, X. Yue, and S. Zhou. A positivity-preserving, energy stable and convergent numerical scheme for the Poisson-Nernst-Planck system. *Math. Comput.*, 90:2071–2106, 2021.

[32] C. Liu, C. Wang, S. Wise, X. Yue, and S. Zhou. A second order accurate numerical method for the Poisson-Nernst-Panck system in the energetic variational formulation. *J. Sci.. Comput.*, 97:23, 2023.

[33] Q. Liu, J. Jing, M. Yuan, and W. Chen. A positivity-preserving, energy stable BDF2 scheme with variable steps for the Cahn–Hilliard equation with logarithmic potential. *J. Sci. Comput.*, 95:1–39, 2023.

[34] Z. Liu and X. Li. The exponential scalar auxiliary variable (E-SAV) approach for phase field models and its explicit computing. *SIAM J. Sci. Comput.*, 42:B630–B655, 2020.

[35] J. Park, A. Salgado, and S. Wise. Benchmark computations of the phase field crystal and functionalized Cahn-Hilliard equations via fully implicit, nesterov accelerated schemes. *Commun. Comput. Phys.*, 33:367–398, 2023.

[36] J. Shen, J. Xu, and J. Yang. The scalar auxiliary variable (SAV) approach for gradient flows. *J. Comput. Phys.*, 353:407–416, 2018.

[37] T. Tang, X. Wu, and J. Yang. Arbitrarily high order and fully discrete Extrapolated RK–SAV/DG schemes for Phase-field Gradient flows. *J. Sci. Comput.*, 93(2):1–23, 2022.

[38] C. Wang and S. Wise. An energy stable and convergent finite-difference scheme for the modified phase field crystal equation. *SIAM J. Numer. Anal.*, 49:945–969, 2011.

[39] K. Wang, Y. Hao, Y. Wang, J. Chen, L. Mao, Y. Deng, J. Chen, S. Yuan, T. Zhang, J. Ren, and W. Liao. Functional hydrogels and their application in drug delivery, biosensors, and tissue engineering. *Int. J. Polym. Sci.*, 2019:3160732, 2019.

[40] W. Wang and C. Xu. A class of efficient high-order time-stepping methods for the anisotropic phase-field dendritic crystal growth model. *J. Comput. Appl. Math.*, 453:116161, 2025.

[41] S. Wise. Unconditionally stable finite difference, nonlinear multigrid simulation of the Cahn-Hilliard-Hele-Shaw system of equations. *J. Sci. Comput.*, 44:38–68, 2010.

[42] Z. Xu and H. Zhang. Stabilized semi-implicit numerical schemes for the Cahn-Hilliard-like equation with variable interfacial parameter. *J. Comput. Appl. Math.*, 346:307–322, 2019.

[43] X. Yang. Linear, first and second-order, unconditionally energy stable numerical schemes for the phase field model of homopolymer blends. *J. Comput. Phys.*, 327:294–316, 2016.

[44] M. Yuan, W. Chen, C. Wang, S. Wise, and Z. Zhang. An energy stable finite element scheme for the three-component Cahn-Hilliard-type model for macromolecular microsphere composite hydrogels. *J. Sci. Comput.*, 87(3):1–30, 2021.

[45] M. Yuan, W. Chen, C. Wang, S. Wise, and Z. Zhang. A second order accurate in time, energy stable finite element scheme for the Flory-Huggins-Cahn-Hilliard equation. *Adv. Appl. Math. Mech.*, 14(6):1477–1508, 2022.

[46] D. Zhai and H. Zhang. Investigation on the application of the TDGL equation in macromolecular microsphere composite hydrogel. *Soft Matter*, 9(3):820–825, 2013.